Mineralogy and crystallization patterns in conodont bioapatite from first occurrence (Cambrian) to extinction (end-Triassic)~~Mineralogy and crystallization pattern in conodonts: changes in bioapatite through the stratigraphic breadth of the conodont fossil record~~

Luca Medici[a], Daniele Malferrari[b], Martina Savioli[b], Annalisa Ferretti[b,*]

[a]*National Research Council of Italy, Institute of Methodologies for Environmental Analysis, C.da S. Loja–Zona Industriale, I–85050 Tito Scalo (Potenza), Italy*

[b]*Department of Chemical and Geological Sciences, University of Modena and Reggio Emilia, Via Campi 103, I–41125 Modena, Italy*

[*] Corresponding author.

E-mail addresses: luca.medici@imaa.cnr.it (L. Medici), daniele.malferrari@unimore.it (D. Malferrari), martina.savioli@unimore.it (M. Savioli), ferretti@unimore.it (A. Ferretti).

ABSTRACT

Bioapatite represents an important acquisition in the evolution of life, both in the seas and ~~over the~~on land~~s~~. Vertebrates applied calcium-phosphate biominerals to grow their skeletal support and to shape their teeth, while some invertebrates sheltered their soft parts within apatite shells. Conodonts were the first among vertebrates to experiment with skeletal biomineralization ~~with~~ of tooth-like elements in their feeding apparatus. Spanning a time record of over 300 million years, they offer a unique tool to test possible variation in bioapatite structure from the experimentation of a very primitive biomineralization type to a more evolute pattern just before ~~getting~~ going extinct. X-ray microdiffraction carried out through an X-ray micro-diffractometer, integrated with environmental scanning electron microscopy coupled with

chemical microanalyses (ESEM-EDX), has been applied in this study to investigate conodont ~~structural investigation~~element crystal structure throughout the entire stratigraphic range of ~~conodonts~~these organisms. In particular, bioapatite crystallographic cell parameters have been calculated for about one hundred conodont elements ranging from the late Cambrian to the Late Triassic. Resulting data clearly indicate two distinct distribution plots of cell parameters for paraconodonts and euconodonts. In contrast, age, taxonomy, geographic provenance and CAI do not affect the dimension of the bioapatite crystal cells. Conodont bioapatite crystallographic cell parameters have been compared with cell parameters resulting from phosphatic/phosphatized material (ostracodes, brachiopods, bryozoans, and fish teeth) present in the same residues producing conodonts. Resulting values of the cell parameters are, in general, mainly correlated with the type of organisms even if, for some of them, a correlation also with age cannot be completely ruled out. According to our data, primary bioapatite appears to imprint a key ~~role~~ signature ~~in~~ on fossil crystal-chemistry (crystal structure and major chemical element contents), while the contribution of fossilization and diagenetic processes seems less relevant.

Keywords: Paraconodonts; euconodonts; microdiffraction; cell parameters; biomineralization.

1. Introduction

Several present and fossil organisms, among both invertebrates and vertebrates, share the use of bioapatite for the formation of their mineralized structures. Bioapatite has peculiar features that make it suitable to act as a structural support for the body (skeleton), to allow mechanical grinding (teeth), and to provide protection for the soft tissues (e.g., shell in brachiopods and skull of vertebrates) (Kallaste and Nemliher, 2005; Pasteris et al., 2008; Liu et al., 2013). Furthermore, bioapatite is an important reserve for phosphorus, a fundamental element for life that is also present ~~also~~ in biological molecules such as DNA, RNA and many proteins, and is one of the main components of ATP (adenosine triphosphate), an essential molecule for the metabolism of living organisms.

Biomineralized structures in biological systems are made up of an organic and an inorganic component. The latter is typically nanocrystalline (10^{-9} m), with nanometric assemblies of atoms with dimensions ranging from ions (10^{-10} m) to macroscopic forms (Banfield and Zhang, 2001). However, there are significant differences between teeth and bones. Teeth are in fact provided with cells completely different from those involved in ossification processes, being odontoblasts specialized in the dentin formation process and ameloblasts in the formation of the enamel. Dentin consists of collagen and nanocrystals of bioapatite, and it is not subject to remodeling during the lifetime of the individual. Mature enamel contains only 2% of proteins and bears bioapatite crystals significantly larger (up to 1000 times greater) than in bones. These differences probably reflect the adaptive capacity of vertebrates that parallels changes imposed by evolution (LeGeros and LeGeros, 1984; Mann, 2001; Skinner, 2005; Glimcher, 2006).

From the crystal-chemical point of view, apatite crystallizes in the hexagonal system and its crystallographic cell parameters, which define the geometry of the crystal lattice in three dimensions by the two parameters *a* (base) and *c* (height), vary in size in close correlation with the isomorphic iso- and hetero-valent substitutions that may occur in the various coordination sites (Hughes et al., 1989) that, additionally, impart distinctive features to bones and teeth as well. For example, there is a close correlation between the solubility of bioapatite and the partial substitution of the phosphate anion by carbonate. It is not accidental that teeth, more subject to the attack of acids, contain much less carbonate than bones in order to be less soluble. Moreover, there is an inverse proportionality ratio between concentration of carbonate and hydroxyl ions in bioapatite, as the substitution of phosphate $(PO_4)^{3-}$ with carbonate $(CO_3)^{2-}$ is counterbalanced by removal of calcium from the lattice and limiting the concentration of hydroxyl ions. As a consequence of these substitutions, the lattice is distorted and crystal growth interrupted (i.e., small sized crystals are formed). The first direct consequence is a drastic increase of the ~~surface~~ surface ~~to~~ to volume ratio and, thus, of the reactivity toward external molecules (Cazalbou et al., 2004; Wopenka and Pasteris, 2005; Glimcher, 2006; Boskey, 2007).

The effects of these chained events significantly affect the overall biomineralization process. Bioapatite crystal formation is, in fact, ruled by appropriate nucleation or crystallization inhibitors and crystal growth depends on the presence of biological fluids saturated with hydroxyapatite and possibly also various trace

elements that can be incorporated within the bioapatite frame (Skinner, 2005; Pasteris et al., 2008). When such inhibitors are removed, mineral growth occurs only from extracellular fluids, whose composition reflects the surrounding environment. Hence several ~~researches~~studies, involving bioapatite as a biological and/or environmental marker, have been carried out on fossil remains or Recent organisms (see Keenan, 2016 for a comprehensive review).

This paper focuses on conodonts, ~~who~~ which dominated the ancient oceans for over 300 million years from the Cambrian to the Triassic. Being extinct, it is not possible to obtain reliable information about their original composition and structure as the elements have undergone fossilization and diagenesis. Conodonts, for a long time considered enigmatic, represent an extinct group of jawless vertebrates, that were the first among the group to experiment skeletal biomineralization with tooth-like elements in their feeding apparatus (Martínez-Pérez et al., 2014). These elements, ranging in average size from 0.1 to 5 mm, consist of bioapatite with a francolite-like structure, and are arranged in a bilaterally-symmetrical apparatus within the cephalic part of the animal. Conodonts, owing to their rapid evolution and diversity of habitats, represent a fundamental biostratigraphical tool within carbonate depositional environments. Moreover, as bioapatite may archive sea water chemistry information, their chemical composition encourages palaeo-environmental investigations on ocean geodynamics and climates (Holmden et al., 1996; Trotter et al., 1999; Wenzel et al., 2000).

In the face of these advantages offered by conodont chemical composition, it seems that fossilization and diagenetic processes can affect some trace element incorporation following the biomineralization process. For example, Trotter and Eggins (2006), through comparative analyses of contemporaneous bioapatites and Holocene and Recent fish material, found a linear relationship~~s~~ between their respective REE, Y, Pb, Th, and U incorporations, with repercussions for their possible liability to diagenesis. A similar argument also applies to vertebrate enamel which, in general, is subject to isomorphic substitutions much less than other mineralized vertebrate tissues (Kohn et al., 1999; Trueman and Tuross, 2002).

Notwithstanding the numerous ~~researches~~ studies that accounted for ~~take into consideration~~ trace element (and isotope) incorporations in conodont bioapatite, little or nothing ~~regards~~ regarding the structural variations of bioapatite in conodont elements has been published. In fact it has been widely

demonstrated that isomorphic substitutions of major elements in apatite significantly affect the dimension of cell parameters (McConnell, 1973; Hughes et al., 1989; Hughes and Rakovan, 2002; Rodríguez-Lorenzo et al., 2003). Conversely, their measure can provide a nice approximation of the quantitative chemical composition of major elements that, in conodonts, is not easily measurable due to their small size and a lack of proper certified analytical standards with a phosphatic matrix. For example, it has been observed that the cell parameter *a* calculated for a pure fluorapatite (obtained by synthesis) is significantly lower than that of natural bioapatites which contain both hydroxyl and carbonate ions. Likewise, a progressive decrease of the same cell parameter in a continuous series of crystals reflects progressive substitutions of hydroxyl with fluorine (Hughes and Rakovan, 2002).

In this paper we measure and compare bioapatite crystallographic cell parameters in conodonts of different age (Cambrian to Triassic), taxonomic assignment, geographic provenance and CAI. Furthermore, cell parameters of conodont bioapatite are compared with those of coeval phosphatic or phosphatized fossils ~~detected~~ recovered from the same residue resulting from conodont preparation (i.e., brachiopods, bryozoans, fish teeth, and ostracodes). The output of the comparison will be related to a possible interference of fossilization and diagenesis after biomineralization. As demonstrated (Ferretti et al., 2017), the calculation of the cell parameters of a single conodont element can be successfully achieved through the employment of micro X-ray diffraction (μ-XRD) measurements which allow to obtain *in-situ* diffraction patterns.

2. Material and methods

2.1. Study materials~~Material under investigation~~

Material ~~here~~ investigated herein derives from conodont collections organized at the University of Modena and Reggio Emilia (IPUM Collection) in his long career by Enrico Serpagli, from material prepared by one of us (AF) in her study on Late Ordovician faunas as well as from specimens kindly provided by other conodont workers. A conodont assemblage of about one hundred elements (Table 1), spanning in age from

the Cambrian to the Triassic (Fig. 1) and including both paraconodonts and euconodonts (Fig. 2), was investigated in this paper. Material results from standard conodont processing techniques.

In order to make comparisons between the bioapatite signal of the conodont elements and those of other fossil organisms, the same analytical procedure was applied to other phosphatic/phospatized organisms selected from the same residues producing conodonts. In this way the investigation has included brachiopods, bryozoans, ostracods and fish teeth (Table 2; Fig. 3).

All analyzed material is housed in the "Palaeontological Collections of the University of Modena and Reggio Emilia: under accession prefix IPUM" at the Department of Chemical and Geological Sciences, University of Modena and Reggio Emilia, Modena, Italy.

2.2 SEM/ESEM microscopy

Conodonts elements and associated phosphatic ~~associated~~ fossils were initially analyzed and photographed under optical and electron microscopy. For non-conodont material, the presence of bioapatite was preliminarily tested. Specimens were mounted on aluminum stubs previously covered with carbon-conductive adhesive tape. Au-coated and non-coated elements were observed using an Environmental Scanning Electron Microscope (ESEM) FEI ESEM-Quanta 200, equipped with an Oxford EDX INCA 300 X-ray energy dispersive spectrometer and by a Scanning Electron Microscope (SEM) Nova NanoSEM FEI 450 equipped with a X-EDS Bruker QUANTAX-200 detector. ESEM observations were performed in high and low vacuum (low vacuum brackets 1 and 0.5 Torr) with an accelerating voltage between 5 and 25 keV for imaging and between 5 and 15 keV for elemental analyses. SEM observations were in high vacuum with an accelerating voltage between 15 and 25 keV for imaging and between 15 and 25 keV for elemental analyses.

2.3. X-ray microdiffraction (μ-XRD)

X-ray diffraction measurements were carried out with a micro X-ray diffractometer. This instrument is extremely versatile and allows the non-destructive study of structural properties of the material such as, for example, the mineralogical composition of the crystalline phases, the degree of crystallinity, the size of crystallites, the detection of preferential orientation, etc., with the same accuracy obtainable with conventional diffractometers, but with the advantage of detecting measurements on very small portions of the sample and, thus, on small-sized fossils. Here, µ-XRD measurements were performed on elements mounted on small plane surfaces. Data were acquired using a Rigaku D/MAX RAPID diffraction system, operating at 40 kV and 30 mA equipped with a Cu*K*α source, curved-image-plate detector, flat graphite monochromator, variety of beam collimators, motorized stage and microscope for accurate positioning of the sample. Measurements were performed in reflection mode using a 300-µm collimator and collection times of 30 minutes and by varying the Omega and Phi angles between one sample and the other to fit with the instrument geometry and thus to obtain a significant number of diffraction effects with a maximized ~~signal~~ signal-~~to~~ to-noise ratio. The µ-XRD data were collected as two-dimensional images and then converted into 2θ-I profiles using the Rigaku R-AXIS Display software. A 300-µm collimator was suitable to obtain mean values of bioapatite cell parameters representative of the conodont elements in their wholeness.

Even ~~if~~ though a previous ~~research~~ study demonstrated that apatite overgrowth perfectly replicates the original structure (Ferretti et al., 2017), when possible each point was selected ~~avoiding~~ to avoid analyses on newly formed crystals. After measurement, unit-cell parameters were refined using UnitCell software (Holland and Redfern, 1997). All diffraction spots shown in the two-dimensional images were excluded due to the fact that they were related~~because due~~ to single crystals (Ferretti et al., 2017).

Optical microscopy and ESEM-EDX analyses were performed at the Scientific Instruments Facility (CIGS) of the University of Modena and Reggio Emilia (Modena, Italy), whereas X-ray diffraction measurements were made at the Institute of Methodologies for Environmental Analysis of the National Research Council of Italy of Tito Scalo (Potenza, Italy).

3. Results

3.1. Conodont faunal data

A collection of over one hundred conodont elements spanning in age from the late Cambrian to the Late Triassic and including both paraconodonts and euconodonts was ~~used for our purposes~~analyzed in this study. Elements were carefully selected ~~mostly~~ and most were from well-known and published sequences biostratigraphically firmly constrained in order to refer to specific time-frames. Only specimens with a good preservation state were analyzed. CAI covered ~~by~~ of our conodont fauna ranges from 1 to 6.

For a specific time frame (Late Ordovician; *Amorphognathus ordovicicus* Zone), elements occupying different positions in the same apparatus were processed in order to test possible contrasting signals. Pa, Pb and Sd elements of *Amorphognathus* sp., Pa and Sd elements of *Sagittodontina robusta* Knüpfer, 1967, and M and Sc elements of *Hamarodus brevirameus* (Walliser, 1964) were investigated for this purpose. Furthermore, results from the widely-distributed taxa *Amorphognathus* sp. and *Scabbardella altipes* (Henningsmoen, 1948) were compared ~~in~~ from three geographic areas: Sardinia (Domusnovas Formation, Italy; Ferretti and Serpagli, 1999) and Normandy (Vaux Limestone, France; Ferretti et al., 2014a) located along the peri-Gondwana margin and Westmorland (Keisley Limestone, UK; Bergström and Ferretti, 2015) located in Avalonia. For a more global assessment of the Late Ordovician conodont faunas, refer to Ferretti et al. (2014b).

3.1.1. ESEM and SEM characterization

Conodont elements were preliminarily investigated in order to monitor distribution of major elements. Environmental scanning electron microscopy coupled with microanalyses (SEM/ESEM-EDX) was applied to the entire surface of the conodont specimens, with special attention to detect variations through the element wall thickness. Broken elements were carefully analyzed and scanned for this purpose. Maps of major element (P, Ca, F, C, Cl, K, Na, Ba, Fe, Pb, S) distribution do not vary significantly through the element wall, both for paraconodonts (Fig. 4A) and euconodonts (Fig. 4B). These findings support the presence of the same carbonate-fluoroapatite in the conodont element.

214

215 *3.1.2. μ-XRD measurements and cell parameter refinements*

216 Table SI–1 reports calculated cell parameters for conodonts (Table SI–1a) and non-conodonts (Table SI–
217 1b) listed in Tables 1–2. If analyzed globally, our data enhance an overall considerable dispersion of the cell
218 parameter *a* of the bioapatite. The cell parameter *c*, differently, appears to be highly variable among the
219 euconodonts (Table S1a), and more stable in the other fossil groups, in particular paraconodonts (Table
220 S1a) and brachiopods (Table S1b).

221 Selected data are plotted and discussed in the following sections.

222 Figure 5 plots the bioapatite crystallographic cell parameters *c vs a* for euconodonts and paraconodonts.
223 It is remarkable that paraconodonts and euconodonts clearly occupy two different and ~~not~~ non-overlapping
224 fields of the plot. More in detail, the comparison clearly highlights that: i) the cell parameter *a* is smaller in
225 paraconodonts than in euconodonts and it ranges between 9.337(6) and 9.392(6) (Table S1a, specimens
226 A14 and A21, respectively); ii) values of the cell parameter~~s~~ *c* of all paraconodonts are very close to the
227 highest values of *c* of the euconodont~~s,~~ that ranges between 6.857(6) and 6.911(2) (Table S1a, specimens
228 A1 and A89, respectively). Figure 6 plots the bioapatite crystallographic cell parameters *c vs a* for
229 conodonts according to their age, spanning from the late Cambrian (Guzhangian) to the Late Triassic
230 (Carnian). It is ~~well~~ highly evident that age does not affect cell parameter distribution. In fact, from a ~~close~~
231 chronological point of view, some values of the cell parameter *a* calculated for the ~~most recent~~youngest
232 euconodonts (Carboniferous and Triassic) are surprisingly much closer to Cambrian paraconodonts than to
233 Ordovician euconodonts. Figure 7 plots the bioapatite crystallographic cell parameters *c vs a* for selected
234 Late Ordovician conodonts according to their taxonomic assignment (Fig. 7A) and geographic area (Fig. 7B).
235 No correlation is evident in ~~both~~ either plots: neither taxonomy (including position occupied within the
236 apparatus architecture) nor geographic location appear to influence cell parameter values.

237

238 *3.2. Other phosphatic fauna (OPF)*

239

Phosphatic/phosphatized material was picked exactly from the same residues that had produced the ~~analyzed~~ conodont elements that were analyzed, in order to detect additional bioapatite signals and to exclude effects of diverse preparation technique and diagenesis. Well preserved phosphatized ostracodes (Fig. 3G–H, L) and undetermined material (Fig. 3F, K) were picked from the same late Cambrian residue so to offer possible comparison with paraconodonts. A wider age range was covered by the analyzed brachiopods (Fig. 3A–C), spanning from the Early Ordovician to the Early Devonian. Particular ~~attention~~ effort was ~~reserved~~ made to document brachiopods from the three Late Ordovician areas (Sardinia, Normandy and Westmoreland) investigated in detail also with conodonts. Only Late Ordovician bryozoans (Fig. 3D–E), but from three geographic sectors, were processed for investigation. Finally, a few fish teeth (Fig. 3I–J) from Upper Triassic residues were measured.

The presence of bioapatite was preliminarily tested by ESEM and SEM techniques so as to exclude non-phosphatic material. No further chemical detailed analysis was attempted.

3.2.1. µ-XRD measurements and unit cell parameter refinements

Figure 8 reports bioapatite crystallographic cell parameters for all analyzed OPF. For simplicity, the age-average values of cell parameters calculated for conodonts are reported as well. Main terms of the comparison are: i) values of the cell parameter *a* calculated for all the OPF are generally lower (or, at least, very close) than those calculated for euconodonts, with the exception of a Late Triassic fish tooth (specimen A47; Norian); ii) on the opposite, values of cell parameter *c* calculated for all the OPF are significantly higher (or, at least, very close) than those calculated for euconodonts, with the exception of a Late Ordovician brachiopod (specimen A55; Katian); iii) late Cambrian OPF (ostracodes and undetermined material) share similar values of both cell parameters with paraconodonts, with the exception of an ostracod (specimen A94; Paibian); iv) similar values were calculated also for Early Devonian (Lochkovian) brachiopods and a Late Triassic (Carnian) fish tooth.

All results will be further discussed below. However, any conclusion from OPF should be regarded as preliminary since the number of analyzed OPF specimens is significantly lower than conodonts and because

we could preliminarily test provenance effects on cell parameters only for bryozoans and brachiopods and age only for brachiopods.

4. Discussion

Bioapatites are generally classified as francolites [$Ca_5(PO_4, CO_3)_3F$)] or as dahllites [$Ca_5(PO_4, CO_3)_3(OH)$]. From a strict mineralogical point of view, these are no longer valid nomenclature forms (discredited by the IMA in 2008) as carbonate is not the dominant species in tetrahedral isomorphic substitutions (type B substitutions) (Wopenka and Pasteris, 2005). Moreover, numerous ~~researches~~ studies carried out ~~so far~~to-date (see Liu et al., 2013 for a review) have shown that many other isomorphic substitutions occur in bioapatites and, in consequence, the chemical formulas of francolite and dahllite cannot be considered completely exhaustive ~~of~~ for the composition of these biomaterials. As mentioned in the Introduction, isomorphic substitutions of major elements in apatite significantly affect crystallographic cell parameter dimensions. For example, substitutions of $(CO_3)^{2-}$ for $(PO_4)^{3-}$ results in an increase of the cell parameter *c* and a contraction of the cell parameter *a*, whereas $(CO_3)^{2-}$ for $(OH)^{-}$ substitution produces the opposite results (LeGeros, 1981). Therefore, even if ~~to~~ to-date there is no evidence that francolite and dahllite can be considered as the end-members of a continuous solid solution, it is unquestionable that the measurement of cell parameters can provide a nice approximation of major element chemical composition. This approach could be mandatory when both the presence of the C element and small size of the sample prevents a more detailed chemical characterization than semi-quantitative EDS or EDX techniques.

Nemliher et al. (2004) combined X-ray diffraction on powdered sample and chemical EDX measurements on fragments of Recent fish and marine mammal skeletons, phosphatic brachiopods and oceanic phosphorites. Data were compared with fossil material and phosphorites of Cretaceous, Miocene and Holocene age. The authors observed a reduction of the cell parameter *a* in fossil material and related this both to the increase of carbonate content and to the decrease in the hydroxyl-ion content subsequent to the recrystallization of apatite. More specifically, they proposed that the substitutions of OH with F are contextual to the progressive decrease in cell volume, evidence that also suggests that these substitutions

do not significantly affect cell parameter *c*. Zhang et al. (2017), through a multi-analytical approach combining Raman spectroscopy, high resolution X-ray diffraction and chemical analyses on well-preserved Ordovician coniform conodonts from South China, documented several chemical substitutions occurring during diagenesis ~~and affecting differently~~that affect conodont tissue types (albid and hyaline crown, and basal body)~~, differences~~ differently. Such observations were previously highlighted by Trotter et al. (2007) in their examination of ~~which studied~~ hyaline and albid~~e~~ crown tissues using transmission electron microscopy.

The absence of significant correlation in our euconodonts between bioapatite cell parameters and taxonomic assignment, age, and geographic provenance of the elements supports the hypothesis that isomorphic substitutions are not exclusively correlated with the age of the fossil. Triassic elements are, in fact, much more deviated compared to the Ordovician ones (Fig. 7). On the other hand~~opposite~~, euconodont cell parameters define a higher range of values than paraconodonts (Fig. 5), even if Ordovician euconodonts are closer in age to paraconodonts than to Early Triassic euconodonts. The existence of two clearly separate distribution fields of cell parameters, one for paraconodonts and one for euconodonts, is further strengthened plotting values of bioapatite cell volume (Fig. SI–1). Again, two distinct distributions appear, one for paraconodonts and one for euconodonts. These results improve the knowledge of these elements which were previously studied and distinguished using synchrotron radiation X-ray tomographic microscopy to characterize and compare the microstructure of morphologically similar euconodont and paraconodont elements (Murdock et al., 2013).

Transformation of an original bioapatite could also occur by dissolution/recrystallization processes or by metasomatic substitutions. Dissolution/recrystallization drives to the formation of large-size crystals with high crystallinity, whereas metasomatic substitutions normally lead to a reduction of the crystallinity and do not affect crystal size. Notwithstanding ~~of~~ which ~~between~~ of the two ~~mentioned~~ is the main promoter of the transformation, there is ~~a~~ general agreement that temperature should favor isomorphic substitution. By restricting the observation to euconodonts, it was thus surprising to find no significant correlation between cell parameters and CAI (Fig. SI–2). Similar conclusions are supported by Zhang et al. (2017) by the

analysis of conodonts exhibiting CAI of 1-3, but with no significant relationship between CAI and chemical composition, Raman spectroscopic features, and crystallinity.

Comparison ~~between~~ of our data and those available in similar studies on conodonts (Fig. SI–3) provides a foremost endorsement of our interpretation. Unfortunately, conodont cell parameters available in the literature are extremely scarce. With the exception of those reported in our previous paper (Ferretti et al., 2017) and here considered, to our knowledge only two researches (Pietzner et al., 1968; Nemliher and Kallaste, 2012) provide this information. Results from Pietzner et al. (1968) were not plotted as information about measurements, and data management are missing. Nemliher and Kallaste (2012) applied an experimental approach, different from ours, but that undoubtedly provides us a~~n~~ useful comparison tool. ~~The~~ In fact, the authors calculated ~~in fact~~ cell parameters from X-ray spectra measured on powders produced grinding various specimens of different taxa belonging to different biozones (ranging from the Early Ordovician to the Silurian). Detected cell parameters could therefore be considered as an average value representative of each biozone. Figure SI–3 shows that there is a nice agreement with our data, including average values calculated for Ordovician elements, and those from the cited authors.

FA ~~f~~urther support ~~to~~ of the absence of a close relationship between cell parameter values and age/geographic provenance is provided by comparing signals of conodonts and other phosphatic fauna (OPF) ~~(~~(Fig. 8). In fact, excluding the out of range cell parameter values above mentioned among OPF (specimens A47 and A55), remaining data could be better sorted considering the fossil group rather than its age or locality.

Lack of additional material does not allow ~~to formulate~~ definitive conclusions to be formulated without speculation~~;~~. ~~however~~However, if our preliminary data ~~will be~~are confirmed by further measurements on larger and more varied faunal collections, including also Recent material and with diverse preservation (Ferretti et al., 2012), it appears that primary biomineralization ~~appears to be able to~~ provides an indelible footprint, only mediated by fossilization and diagenetic processes.

5. Conclusions

This research has added to routine morphological and chemical qualitative characterization, achievable through optical and electronic microscopy, ~~also~~ by integrating a crystallographic approach~~,~~ based on X-ray microdiffraction (µ-XRD)~~,~~ to gain enhanced structural information ~~on~~ about conodonts and other bioapatite fossils. Microdiffraction measurements, recently introduced in conodont studies by our research group, is, in fact, a powerful tool ~~to~~ for obtaining crystallographic information when dealing with small-sized samples like conodont elements. Moreover, µ-XRD is a non-~~distructive~~ destructive ~~and mandatory~~ technique ~~when~~ for dealing with ~~unreplaceable~~ irreplaceable material. The methodological approach and the results here obtained were additionally strengthened by comparison with data from the literature that had been ~~data~~ obtained through conventional methods (X-ray powder diffraction) that parallel our findings.

As reported in the literature, bioapatite crystallographic cell parameters strongly depend on different isomorphic substitutions. Our data reveal that cell parameters calculated for paraconodonts significantly differ from those derived ~~with~~ for euconodonts. ~~Paraconodonts~~ In fact, paraconodonts bear ~~in fact~~ smaller cell parameters *a* and higher cell parameters *c*, very close to the highest values of *c* of euconodonts. Moreover, cell parameters calculated for both paraconodonts and euconodonts appear to be independent ~~from~~ of age, taxonomic assignment, geographic provenance and, for euconodonts, CAI (i.e., temperature). Other phosphatic/phosphatized material from the same residues producing conodonts are characterized by values of the cell parameters that, in a preliminary way, appear to be mainly correlated with the type of organism even if, for some of them, a correlation also with age cannot be completely ruled out.

It is, therefore, conceivable that major element content strongly depends not only on fossilization, diagenesis and metasomatism, but mostly on the primary bioapatite composition. In other words, from a close crystal-chemical point of view, it is not possible to unequivocally conclude, for example, that the cell parameter *a*, smaller in paraconodonts than in euconodonts, is the direct consequence of a sort of "francolitization" process (i.e., the formation, for progressive and successive isomorphic substitutions, of the end-member francolite that, as already pointed out, was never proved) during fossilization and/or diagenesis.

Acknowledgements

A long list of friends provided us conodont material and taxonomic assignment of the specimens. Enrico Serpagli created, over the course of ~~in~~ his superb career, an invaluable conodont collection at the University of Modena and Reggio Emilia for future studies. Claudia Spalletta, Maria Cristina Perri, Michele Mazza, Manuel Rigo and Carlo Corradini are greatly acknowledged for their invaluable support. We are especially grateful to Massimo Tonelli (University of Modena and Reggio Emilia – Scientific Instruments Facility) for SEM/ESEM expertise.

The Editor-in-Chief, Thomas J. Algeo, the Guest Editors, Alyssa Bancroft and John Repetski, and two anonymous reviewers provided valuable comments during the course of this study. Financial support was provided under grant FAR 2016 PAsTIME, University of Modena and Reggio Emilia. This paper is a contribution to IGCP Project 653 “The onset of the Great Ordovician Biodiversity Event”.

References

Banfield J.F., Zhang H., 2001. Nanoparticles in the environment. Rev. Mineral. Geochem. 44(1), 1–58.

Bergström, S.M., Ferretti, A., 2015. Conodonts in the Upper Ordovician Keisley Limestone of northern England: taxonomy, biostratigraphical significance and biogeographical relationships. Pap. Palaeont. 93, 1–32.

Boskey, A., 2007. Mineralization of bones and teeth. Elements 3, 385–391.

Cazalbou, S., Combes, C., Eichert, D., Rey, C., 2004. Adaptive physico-chemistry of bio-related calcium phosphates. J. Mater. Chem. 14, 2148–2153.

Chlupáč, I., Kříž, J., Schönlaub, H.P., 1980. Field Trip E, ECOS II, Barrandian. Abh. Geol. Bundesanst. 35, 147–180.

Cohen, K.M., Finney, S.C., Gibbard, P.L., Fan, J.-X., 2013; updated 2018. The ICS international chronostratigraphic chart. Episodes 36, 199–204.

Farabegoli, E., Perri, M.C., 1998. Scythian and Anisian conodonts from the Sotto le Rive section (Southern Alps, Italy). Giorn. Geol. 60, 254–259.

Ferretti, A., Bergström, S.M., Barnes, C.R., 2014b. Katian (Upper Ordovician) conodonts from Wales. Palaeontology 57(4), 801–831.

Ferretti, A., Cavalazzi, B., Barbieri, R., Westall, F., Foucher, F., Todesco, R., 2012. From black-and-white to colour in the Silurian. Palaeogeogr., Palaeoclimatol., Palaeoecol. 367–368, 505–519.

Ferretti, A., Malferrari, D., Medici, L., Savioli, M., 2017. Diagenesis does not invent anything new: Precise replication of conodont structures by secondary apatite. Sci. Rep. 7 (1), 1624–1632.

Ferretti, A., Messori, A., Bergström, S.M., 2014a. Composition and significance of the Katian (Upper Ordovician) conodont fauna of the Vaux Limestone ("Calcaire des Vaux") in Normandy, France. Est. J. Earth Sci. 63(4), 214–219.

Ferretti, A., Serpagli, E., 1999. Late Ordovician conodont faunas from southern Sardinia, Italy: biostratigraphic and paleogeographic implications. Boll. Soc. Paleont. Ital. 37(2–3), 215–236.

Glimcher, M.J., 2006. Bone: Nature of the calcium phosphate crystals and cellular, structural, and physical chemical mechanisms in their formation. Rev. Mineral. Geochem. 64. 223–282.

Holland, T.J.B., Redfern, S.A.T., 1997. Unit cell refinement from powder diffraction data: the use of regression diagnostics. Mineral. Mag. 61, 65–77.

Holmden, C., Creaser, R.A., Muehlenbachs, K., Bergström, S.M., Leslie, S.A., 1996. Isotopic and elemental systematics of Sr and Nd in 454 Ma biogenic apatites: implications for paleoseawater studies. Earth. Planet. Sci. Lett. 142, 425–437.

Hughes, J.M., Cameron, M., Crowley, K.D., 1989. Structural variations in natural F, OH, and Cl apatites. Am. Mineral. 74, 870–876.

Hughes, J.M., Rakovan, J., 2002. The Crystal Structure of Apatite, Ca5(PO4)3(F,OH,Cl). Rev. Mineral. Geochem. 48. 1– 12.

Kallaste, T., Nemliher, J., 2005. Apatite varieties in extant and fossil vertebrate mineralized tissues. J. Appl. Cryst. 38, 587–594.

Keenan, S.W., 2016. From bone to fossil: A review of the diagenesis of bioapatite. Am. Mineral. 101(9), 1943–1951.

Kohn, M.J., Schoeninger, M.J., Barker, W.W., 1999. Altered states: effects of diagenesis on fossil tooth chemistry. Geochim. Cosmochim. Acta 63(18), 2737–2747.

Kovaçs, S., Papsova, J., Perri, M.C., 1996. New Middle Triassic conodonts of the *Gondolella szabòi-G. trammeri* lineage from the West Carpathian Mts and from the Southern Alps. Acta Geol. Hung. 39(1), 101–128.

LeGeros, R.Z., 1981. Apatites in biological systems. Prog. Cryst. Growth Charact. Mater. 4(1–2), 1–45.

LeGeros, R.Z., LeGeros, J.P., 1984. Phosphate minerals in human tissue. In: Nriagu, J.O., Moore, P.B. (Eds.), Phosphate Minerals. Springer-Verlag, New York, pp. 351–395.

Liu, Q., Huang, S., Pekka Matinlinna, J., Chen, Z., Pan, H., 2013. Insight into Biological Apatite: Physiochemical Properties and Preparation Approaches. BioMed. Research International 929, 7–48.

Mann, S., 2001. Biomineralization: Principles and Concepts in Bioinorganic Materials Chemistry. Oxford University Press, Oxford, pp. 1–198.

Martínez-Pérez, C., Rayfield, E.J., Purnell, M.A., Donoghue, P.C.J., 2014. Finite element, occlusal, microwear and microstructural analyses indicate that conodont microstructure is adapted to dental function. Palaeontology 57(5), 1059–1066.

Mazza, M., Martínez-Pérez, C. 2015. Unravelling conodont (Conodonta) ontogenetic processes in the Late Triassic through growth series reconstructions and X-ray microtomography. Boll. Soc. Paleont. Ital. 54(3), 161–186.

Mazza, M., Rigo, M., Gullo, M., 2012. Taxonomy and stratigraphic record of the Upper Triassic conodonts of the Pizzo Mondello section (Western Sicily, Italy), GSSP candidate for the base of the Norian. Riv. It. Paleont. Strat. 118(1), 85–130.

McConnell, D., 1973. Apatite – its crystal chemistry, mineralogy, utilization and geological and biological occurrences. Applied Mineralogy, Springer-Verlag, Wien, pp. 1–111.

Müller, K.J., Hinz, I. 1991. Upper Cambrian conodonts from Sweden. Fossils & Strata 28, 1–153.

Murdock, D.J.E., Dong, X.-P., Repetski, J.E., Marone, F., Stampanoni, M., Donoghue, P.C.J., 2013. The origin of conodonts and of vertebrate mineralized skeletons. Nature 502, 546–549.

Nemliher, J.G., Baturin, G.N., Kallaste, T.E., Murdmaa, I.O., 2004. Transformation of Hydroxyapatite of Bone Phosphate from the Ocean Bottom during Fossilization. Lithol. Miner. Resour. 39(5), 468–479.

452 Nemliher, J., Kallaste, T., 2012. Conodont bioapatite resembles vertebrate enamel by XRD properties. Est. J.
453 Earth Sci. 61(3), 191–192.
454 Pasteris, J.D., Wopenka, B., Valsami-Jones, E., 2008. Bone and tooth mineralization: why apatite? Elements
455 4(2), 97–104.
456 Perri, M.C., Andraghetti, M., 1987. Permian–Triassic boundary and Early Triassic conodonts from the
457 Southern Alps, Italy. Riv. It. Paleont. Strat. 93 (3), 291–328.
458 Perri, M.C., Spalletta, C., 1998. Latest Devonian and Early Carboniferous conodonts from the Casera
459 Collinetta di Sotto A section (Carnic Alps, Italy). Giorn. Geol. 60, 168–181.
460 Pietzner, H., Vahl, J., Werner, H., Ziegler, W., 1968. Zur chemischen Zuzammensetzung und
461 Mikromorphologie der Conodonten. Palaeontographica 128, 115–152.
462 Rodríguez-Lorenzo, L.M., Hart, J.N., Gross, K.A., 2003. Structural and Chemical Analysis of Well-Crystallized
463 Hydroxyfluorapatites. J. Phys. Chem. B 107, 8316–8320.
464 Skinner, H.C.W., 2005. Biominerals. Mineral. Mag. 69, 621–641.
465 Spalletta, C., Perri, M.C., 1998a. The Frasnian-Famennian boundary at the Pramosio A section (Carnic Alps,
466 Italy). Giorn. Geol. 60, 198–205.
467 Spalletta, C., Perri, M.C., 1998b. Lower Carboniferous conodonts at the Tournaisian/Visean boundary in the
468 Dolina section (Carnic Alps, Italy). Giorn. Geol. 60, 244–253.
469 Szaniawski, H., 1971. New species of Upper Cambrian conodonts from Poland. Acta Palaeontol. Pol. XVI(4),
470 401–413.
471 Trotter, J.A., Eggins, S.M., 2006. Chemical systematics of conodont apatite determined by laser ablation
472 ICPMS. Chem. Geol. 233(3), 196–216.
473 Trotter, J.A., Fitz Gerald, J.D., Kokkonen, H., Barnes, C.R., 2007. New insights into the ultrastructure,
474 permeability, and integrity of conodont apatite determined by transmission electron microscopy.
475 Lethaia 40(2), 97–110.
476 Trotter, J.A., Korsch, M.J., Nicoll, R.S., Whitford, D.J., 1999. Sr isotopic variation in single conodont
477 elements: implications for defining the Sr seawater curve. Boll. Soc. Paleont. Ital. 37(2–3), 507–514.

Trueman, C.N., Tuross, N., 2002. Trace elements of recent and fossil bone apatite. Rev. Mineral. Geochem. 48, 489–521.

Viira, V. 1970. Conodonts of the Varangu Member (Estonian Upper Tremadoc). Eesti NSV Tead. Akad. Toim. Keemia Geol. 19, 224–233.

Wenzel, B., Lécuyer, C., Joachimski, M.M., 2000. Comparing oxygen isotope records of Silurian calcite and phosphate–$\delta^{18}O$ compositions of brachiopods and conodonts. Geochim. Cosmochim. Acta 64(11), 1859–1872.

Wopenka, B., Pasteris, J.D., 2005. A mineralogical perspective on the apatite in bone. Mater. Sci. Eng. C 25, 131–143.

Zhang, L., Cao, L., Zhao, L., Algeo, T.J., Chen, Z.Q., Li, Z., Lv, Z., Wang, X., 2017. Raman spectral, elemental, crystallinity, and oxygen-isotope variations in conodont apatite during diagenesis. Geochim. Cosmochim. Acta 210(1), 184–207.

CAPTION TO FIGURES

Fig. 1. Different time frames investigated in this ~~paper~~ study plotted on the latest version of the International Commission on Stratigraphy Chronostratigraphic Chart (2018/08: http://www.stratigraphy.org/index.php/ics-chart-timescale; see Cohen et al., 2013, updated 2018).

Fig. 2. Some of the conodont elements analyzed in this study. A~~.~~ : *Westergaardodina* sp., late Cambrian, specimen no. A11, IPUM 29101, Västergötland (Sweden); B~~.~~ : *Furnishina alata* Szaniawski, 1971, late Cambrian, specimen no. A18, IPUM 29102, Żarnowiec (Poland); C~~.~~ : *Furnishina* sp., late Cambrian, specimen no. A14, IPUM 29103, Västergötland (Sweden); D~~.~~ : *Paltodus deltifer deltifer* (Lindström, 1955), Early Ordovician, specimen no. A6, IPUM 29104, Öland (Sweden); E~~.~~ : *Hamarodus brevirameus* (Walliser, 1964), M element, Late Ordovician, specimen no. 82, IPUM 29105, Normandy (France); F~~.~~ : *Amorphognathus* sp., Pb element, Late Ordovician, specimen no. A41, IPUM 29106, Sardinia (Italy); G~~.~~ : *Amorphognathus* sp., Pb element, Late Ordovician, specimen no. A27, IPUM 29107, Westmorland (UK);

H–: *Lanea omoalpha* (Murphy and Valenzuela-Ríos, 1999), Early Devonian, specimen no. A2, IPUM 29108, U Topolů (Bohemia); I–: *Rhipidognathus symmetricus* Branson, Mehl and Branson, 1951, Late Ordovician, specimen no. A22, IPUM 29109, Saluda Dolomite (USA); J–: *Scabbardella altipes* (Henningsmoen, 1948), Late Ordovician, specimen no. 45, IPUM 29110, Normandy (France); K–: *Amorphognathus* sp., Pa element, Late Ordovician, specimen no. A98, IPUM 29111, Westmorland (UK); L–: *Zieglerodina planilingua* (Murphy and Valenzuela-Ríos, 1999), Early Devonian, specimen no. A1, IPUM 29112, U Topolů (Bohemia); M–: *Polygnathus decorosus* Stauffer, 1938, Late Devonian, specimen no. A83, IPUM 29113, Carnic Alps (Italy); N–: *Palmatolepis* sp., Late Devonian, specimen no. A82, IPUM 29114, Carnic Alps (Italy); O–: *Gnathodus* sp., Middle Mississippian, specimen no. A78, IPUM 29115, Carnic Alps (Italy); P–: *Branmehla werneri* (Ziegler, 1957), Late Devonian, specimen no. A81, IPUM 29116, Carnic Alps (Italy); Q–: *Palmatolepis triangularis* Sannemann, 1955, Late Devonian, specimen no. A101, IPUM 29117, Texas (USA); R–: *Palmatolepis subperlobata* Branson and Mehl, 1934, Late Devonian, specimen no. A102, IPUM 29118, Texas (USA); S, U–: *Pachycladina obliqua* Staesche, 1964, Early Triassic, specimens no. A87 and A86, IPUM 29119 and IPUM 29121, Dolomites (Italy); T–: unrecognizable fragment, Early Mississippian, specimen no. A77, IPUM 29120, Carnic Alps (Italy); V–: unrecognizable fragment, Middle Triassic, specimen no. A84, IPUM 29122, Dolomites (Italy); W–X–: *Carnepigondolella pseudodiebeli* (Kozur, 1972), Late Triassic, specimens no. A44 and A43, IPUM 29123 and IPUM 29124, Sicily (Italy).

Scale bars correspond to 200 µm.

Fig. 3. Some of the other phosphatic fauna analyzed in this study. A–C–: Brachiopodsbrachiopods, Early Devonian (A) and Late Ordovician (B–C), specimens no. A3, A26 and A36, IPUM 29125–29127, U Topolů (Bohemia), Westmorland (UK) and Sardinia (Italy), respectively; D–E–: Bryozoansbryozoans, Late Ordovician, specimens no. A24 and A61, IPUM 29128 and IPUM 29129, Saluda Dolomite (USA) and Normandy (France), respectively; F, K–: Undetermined undetermined phosphatic material, late Cambrian, specimens no. A95 and A96, IPUM 29130 and IPUM 29135, Västergötland (Sweden); G–H, L–: Ostracodesostracodes, late Cambrian, specimens no. A17, A94 and A93, IPUM 29131, IPUM 29132 and

IPUM 29136, Västergötland (Sweden); I–J: f. Fish teeth, Late Triassic, specimens no. A45 and A46, IPUM 29133 and IPUM 29134, Sicily (Italy).

Scale bars correspond to 500 µm except for G (400 µm) and H, L (300 µm).

Fig. 4. Chemical composition. ESEM image and SEM-EDS elemental maps (P, Ca, F, C, and Cl). A: *Furnishina* sp., late Cambrian, specimen no. A110, IPUM 29137, Västergötland (Sweden). B: *Scabbardella altipes* (Henningsmoen, 1948), Late Ordovician; specimen no. A109, IPUM 29138, Normandy (France).

Scale bars correspond to 200 µm.

Fig. 5. Binary plot of bioapatite crystallographic unit-cell parameters *c vs a* for euconodonts and paraconodonts.

Fig. 6. Binary plot of bioapatite crystallographic unit-cell parameters *c vs a* of conodonts by age.

Fig. 7. Binary plot of bioapatite crystallographic unit-cell parameters *c vs a* of Late Ordovician conodonts by taxonomy (A) and geographic provenance (B).

Fig. 8. Binary plot of bioapatite crystallographic unit-cell parameters *c vs a* for other phosphatic/phosphatized fauna (ostracodes, brachiopods, bryozoans and fish teeth) compared with average values of conodonts by age.

CAPTION TO TABLES

Table 1. Conodont taxa analyzed in the present paper, referred to geographic location/formation, age, and most relevant literature. P: paraconodont; E: euconodont.

557 Table 2. Other phosphatic/phosphatized taxa analyzed in the present paper, referred to geographic
558 location and age.

Mineralogy and crystallization patterns in conodont bioapatite from first occurrence (Cambrian) to extinction (end-Triassic)

Luca Medici, Daniele Malferrari, Martina Savioli, Annalisa Ferretti

Highlights

- Bioapatite crystallographic cell parameters *a* and *c* are variable.
- Bioapatite cell parameters of paraconodonts differ from cell parameters of euconodonts.
- Age, taxonomy, geographic provenance and CAI of conodonts do not influence bioapatite cell parameters.
- Primary bioapatite, only mediated by fossilization and diagenetic processes, rules unit cell parameters.

PARACONODONTS

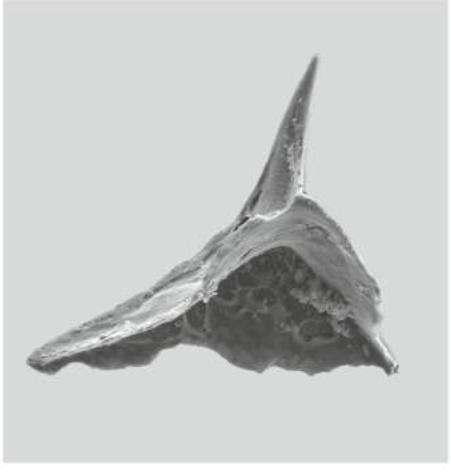

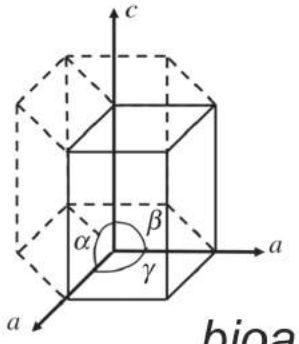

bioapatite

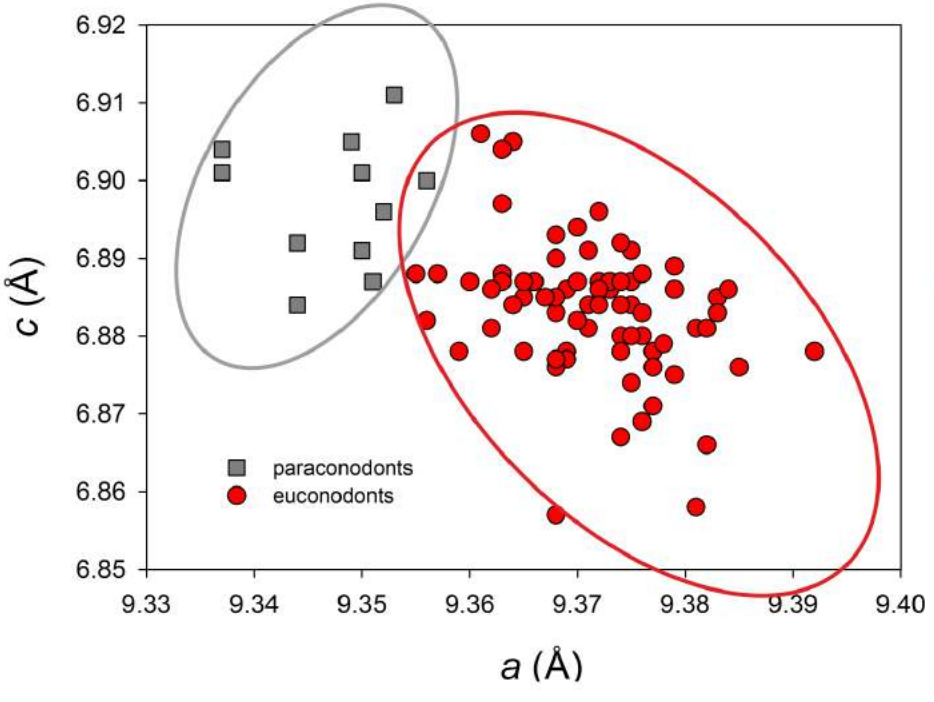

EUCONODONTS

Mineralogy and crystallization patterns in conodont bioapatite from first occurrence (Cambrian) to extinction (end-Triassic)

Luca Medici[a], Daniele Malferrari[b], Martina Savioli[b], Annalisa Ferretti[b,*]

[a]*National Research Council of Italy, Institute of Methodologies for Environmental Analysis, C.da S. Loja–Zona Industriale, I–85050 Tito Scalo (Potenza), Italy*

[b]*Department of Chemical and Geological Sciences, University of Modena and Reggio Emilia, Via Campi 103, I–41125 Modena, Italy*

[*] Corresponding author.

E-mail addresses: luca.medici@imaa.cnr.it (L. Medici), daniele.malferrari@unimore.it (D. Malferrari), martina.savioli@unimore.it (M. Savioli), ferretti@unimore.it (A. Ferretti).

ABSTRACT

Bioapatite represents an important acquisition in the evolution of life, both in the seas and on land. Vertebrates applied calcium-phosphate biominerals to grow their skeletal support and to shape their teeth, while some invertebrates sheltered their soft parts within apatite shells. Conodonts were the first among vertebrates to experiment with skeletal biomineralization of tooth-like elements in their feeding apparatus. Spanning a time record of over 300 million years, they offer a unique tool to test possible variation in bioapatite structure from the experimentation of a very primitive biomineralization type to a more evolute pattern just before going extinct. X-ray microdiffraction carried out through an X-ray micro-diffractometer, integrated with environmental scanning electron microscopy coupled with chemical microanalyses (ESEM-EDX), has been applied in this study to investigate conodont element crystal structure throughout the entire stratigraphic range of these organisms. In particular, bioapatite crystallographic cell parameters have

been calculated for about one hundred conodont elements ranging from the late Cambrian to the Late Triassic. Resulting data clearly indicate two distinct distribution plots of cell parameters for paraconodonts and euconodonts. In contrast, age, taxonomy, geographic provenance and CAI do not affect the dimension of the bioapatite crystal cells. Conodont bioapatite crystallographic cell parameters have been compared with cell parameters resulting from phosphatic/phosphatized material (ostracodes, brachiopods, bryozoans, and fish teeth) present in the same residues producing conodonts. Resulting values of the cell parameters are, in general, mainly correlated with the type of organisms even if, for some of them, a correlation also with age cannot be completely ruled out. According to our data, primary bioapatite appears to imprint a key signature on fossil crystal-chemistry (crystal structure and major chemical element contents), while the contribution of fossilization and diagenetic processes seems less relevant.

Keywords: Paraconodonts; euconodonts; microdiffraction; cell parameters; biomineralization.

1. Introduction

Several present and fossil organisms, among both invertebrates and vertebrates, share the use of bioapatite for the formation of their mineralized structures. Bioapatite has peculiar features that make it suitable to act as a structural support for the body (skeleton), to allow mechanical grinding (teeth), and to provide protection for the soft tissues (e.g., shell in brachiopods and skull of vertebrates) (Kallaste and Nemliher, 2005; Pasteris et al., 2008; Liu et al., 2013). Furthermore, bioapatite is an important reserve for phosphorus, a fundamental element for life that is also present in biological molecules such as DNA, RNA and many proteins, and is one of the main components of ATP (adenosine triphosphate), an essential molecule for the metabolism of living organisms.

Biomineralized structures in biological systems are made up of an organic and an inorganic component. The latter is typically nanocrystalline (10^{-9} m), with nanometric assemblies of atoms with dimensions ranging from ions (10^{-10} m) to macroscopic forms (Banfield and Zhang, 2001). However, there are significant differences between teeth and bones. Teeth are in fact provided with cells completely different from those

54 involved in ossification processes, being odontoblasts specialized in the dentin formation process and
55 ameloblasts in the formation of the enamel. Dentin consists of collagen and nanocrystals of bioapatite, and
56 it is not subject to remodeling during the lifetime of the individual. Mature enamel contains only 2% of
57 proteins and bears bioapatite crystals significantly larger (up to 1000 times greater) than in bones. These
58 differences probably reflect the adaptive capacity of vertebrates that parallels changes imposed by
59 evolution (LeGeros and LeGeros, 1984; Mann, 2001; Skinner, 2005; Glimcher, 2006).

60 From the crystal-chemical point of view, apatite crystallizes in the hexagonal system and its
61 crystallographic cell parameters, which define the geometry of the crystal lattice in three dimensions by the
62 two parameters *a* (base) and *c* (height), vary in size in close correlation with the isomorphic iso- and hetero-
63 valent substitutions that may occur in the various coordination sites (Hughes et al., 1989) that, additionally,
64 impart distinctive features to bones and teeth as well. For example, there is a close correlation between the
65 solubility of bioapatite and the partial substitution of the phosphate anion by carbonate. It is not accidental
66 that teeth, more subject to the attack of acids, contain much less carbonate than bones in order to be less
67 soluble. Moreover, there is an inverse proportionality ratio between concentration of carbonate and
68 hydroxyl ions in bioapatite, as the substitution of phosphate $(PO_4)^{3-}$ with carbonate $(CO_3)^{2-}$ is
69 counterbalanced by removal of calcium from the lattice and limiting the concentration of hydroxyl ions. As
70 a consequence of these substitutions, the lattice is distorted and crystal growth interrupted (i.e., small sized
71 crystals are formed). The first direct consequence is a drastic increase of the surface-to-volume ratio and,
72 thus, of the reactivity toward external molecules (Cazalbou et al., 2004; Wopenka and Pasteris, 2005;
73 Glimcher, 2006; Boskey, 2007).

74 The effects of these chained events significantly affect the overall biomineralization process. Bioapatite
75 crystal formation is, in fact, ruled by appropriate nucleation or crystallization inhibitors and crystal growth
76 depends on the presence of biological fluids saturated with hydroxyapatite and possibly also various trace
77 elements that can be incorporated within the bioapatite frame (Skinner, 2005; Pasteris et al., 2008). When
78 such inhibitors are removed, mineral growth occurs only from extracellular fluids, whose composition
79 reflects the surrounding environment. Hence several studies, involving bioapatite as a biological and/or

environmental marker, have been carried out on fossil remains or Recent organisms (see Keenan, 2016 for a comprehensive review).

This paper focuses on conodonts, which dominated the ancient oceans for over 300 million years from the Cambrian to the Triassic. Being extinct, it is not possible to obtain reliable information about their original composition and structure as the elements have undergone fossilization and diagenesis. Conodonts, for a long time considered enigmatic, represent an extinct group of jawless vertebrates, that were the first among the group to experiment skeletal biomineralization with tooth-like elements in their feeding apparatus (Martínez-Pérez et al., 2014). These elements, ranging in average size from 0.1 to 5 mm, consist of bioapatite with a francolite-like structure, and are arranged in a bilaterally-symmetrical apparatus within the cephalic part of the animal. Conodonts, owing to their rapid evolution and diversity of habitats, represent a fundamental biostratigraphical tool within carbonate depositional environments. Moreover, as bioapatite may archive sea water chemistry information, their chemical composition encourages palaeo-environmental investigations on ocean geodynamics and climates (Holmden et al., 1996; Trotter et al., 1999; Wenzel et al., 2000).

In the face of these advantages offered by conodont chemical composition, it seems that fossilization and diagenetic processes can affect some trace element incorporation following the biomineralization process. For example, Trotter and Eggins (2006), through comparative analyses of contemporaneous bioapatites and Holocene and Recent fish material, found a linear relationship between their respective REE, Y, Pb, Th, and U incorporations, with repercussions for their possible liability to diagenesis. A similar argument also applies to vertebrate enamel which, in general, is subject to isomorphic substitutions much less than other mineralized vertebrate tissues (Kohn et al., 1999; Trueman and Tuross, 2002).

Notwithstanding the numerous studies that accounted for trace element (and isotope) incorporations in conodont bioapatite, little or nothing regarding the structural variations of bioapatite in conodont elements has been published. In fact it has been widely demonstrated that isomorphic substitutions of major elements in apatite significantly affect the dimension of cell parameters (McConnell, 1973; Hughes et al., 1989; Hughes and Rakovan, 2002; Rodríguez-Lorenzo et al., 2003). Conversely, their measure can provide a nice approximation of the quantitative chemical composition of major elements that, in conodonts, is not

easily measurable due to their small size and a lack of proper certified analytical standards with a phosphatic matrix. For example, it has been observed that the cell parameter *a* calculated for a pure fluorapatite (obtained by synthesis) is significantly lower than that of natural bioapatites which contain both hydroxyl and carbonate ions. Likewise, a progressive decrease of the same cell parameter in a continuous series of crystals reflects progressive substitutions of hydroxyl with fluorine (Hughes and Rakovan, 2002).

In this paper we measure and compare bioapatite crystallographic cell parameters in conodonts of different age (Cambrian to Triassic), taxonomic assignment, geographic provenance and CAI. Furthermore, cell parameters of conodont bioapatite are compared with those of coeval phosphatic or phosphatized fossils recovered from the same residue resulting from conodont preparation (i.e., brachiopods, bryozoans, fish teeth, and ostracodes). The output of the comparison will be related to a possible interference of fossilization and diagenesis after biomineralization. As demonstrated (Ferretti et al., 2017), the calculation of the cell parameters of a single conodont element can be successfully achieved through the employment of micro X-ray diffraction (μ-XRD) measurements which allow to obtain *in-situ* diffraction patterns.

2. Material and methods

2.1. Study materials

Material investigated herein derives from conodont collections organized at the University of Modena and Reggio Emilia (IPUM Collection) in his long career by Enrico Serpagli, from material prepared by one of us (AF) in her study on Late Ordovician faunas as well as from specimens kindly provided by other conodont workers. A conodont assemblage of about one hundred elements (Table 1), spanning in age from the Cambrian to the Triassic (Fig. 1) and including both paraconodonts and euconodonts (Fig. 2), was investigated in this paper. Material results from standard conodont processing techniques.

In order to make comparisons between the bioapatite signal of the conodont elements and those of other fossil organisms, the same analytical procedure was applied to other phosphatic/phospatized

organisms selected from the same residues producing conodonts. In this way the investigation has included brachiopods, bryozoans, ostracods and fish teeth (Table 2; Fig. 3).

All analyzed material is housed in the "Palaeontological Collections of the University of Modena and Reggio Emilia: under accession prefix IPUM" at the Department of Chemical and Geological Sciences, University of Modena and Reggio Emilia, Modena, Italy.

2.2 SEM/ESEM microscopy

Conodonts elements and associated phosphatic fossils were initially analyzed and photographed under optical and electron microscopy. For non-conodont material, the presence of bioapatite was preliminarily tested. Specimens were mounted on aluminum stubs previously covered with carbon-conductive adhesive tape. Au-coated and non-coated elements were observed using an Environmental Scanning Electron Microscope (ESEM) FEI ESEM-Quanta 200, equipped with an Oxford EDX INCA 300 X-ray energy dispersive spectrometer and by a Scanning Electron Microscope (SEM) Nova NanoSEM FEI 450 equipped with a X-EDS Bruker QUANTAX-200 detector. ESEM observations were performed in high and low vacuum (low vacuum brackets 1 and 0.5 Torr) with an accelerating voltage between 5 and 25 keV for imaging and between 5 and 15 keV for elemental analyses. SEM observations were in high vacuum with an accelerating voltage between 15 and 25 keV for imaging and between 15 and 25 keV for elemental analyses.

2.3. X-ray microdiffraction (μ-XRD)

X-ray diffraction measurements were carried out with a micro X-ray diffractometer. This instrument is extremely versatile and allows the non-destructive study of structural properties of the material such as, for example, the mineralogical composition of the crystalline phases, the degree of crystallinity, the size of crystallites, the detection of preferential orientation, etc., with the same accuracy obtainable with conventional diffractometers, but with the advantage of detecting measurements on very small portions of the sample and, thus, on small-sized fossils. Here, μ-XRD measurements were performed on elements

mounted on small plane surfaces. Data were acquired using a Rigaku D/MAX RAPID diffraction system, operating at 40 kV and 30 mA equipped with a CuKα source, curved-image-plate detector, flat graphite monochromator, variety of beam collimators, motorized stage and microscope for accurate positioning of the sample. Measurements were performed in reflection mode using a 300-µm collimator and collection times of 30 minutes and by varying the Omega and Phi angles between one sample and the other to fit with the instrument geometry and thus to obtain a significant number of diffraction effects with a maximized signal-to-noise ratio. The µ-XRD data were collected as two-dimensional images and then converted into 2θ-I profiles using the Rigaku R-AXIS Display software. A 300-µm collimator was suitable to obtain mean values of bioapatite cell parameters representative of the conodont elements in their wholeness.

Even though a previous study demonstrated that apatite overgrowth perfectly replicates the original structure (Ferretti et al., 2017), when possible each point was selected to avoid analyses on newly formed crystals. After measurement, unit-cell parameters were refined using UnitCell software (Holland and Redfern, 1997). All diffraction spots shown in the two-dimensional images were excluded due to the fact that they were related to single crystals (Ferretti et al., 2017).

Optical microscopy and ESEM-EDX analyses were performed at the Scientific Instruments Facility (CIGS) of the University of Modena and Reggio Emilia (Modena, Italy), whereas X-ray diffraction measurements were made at the Institute of Methodologies for Environmental Analysis of the National Research Council of Italy of Tito Scalo (Potenza, Italy).

3. Results

3.1. Conodont faunal data

A collection of over one hundred conodont elements spanning in age from the late Cambrian to the Late Triassic and including both paraconodonts and euconodonts was analyzed in this study. Elements were carefully selected and most were from well-known and published sequences biostratigraphically firmly

187 constrained in order to refer to specific time-frames. Only specimens with a good preservation state were
188 analyzed. CAI covered of our conodont fauna ranges from 1 to 6.
189 For a specific time frame (Late Ordovician; *Amorphognathus ordovicicus* Zone), elements occupying
190 different positions in the same apparatus were processed in order to test possible contrasting signals. Pa,
191 Pb and Sd elements of *Amorphognathus* sp., Pa and Sd elements of *Sagittodontina robusta* Knüpfer, 1967,
192 and M and Sc elements of *Hamarodus brevirameus* (Walliser, 1964) were investigated for this purpose.
193 Furthermore, results from the widely-distributed taxa *Amorphognathus* sp. and *Scabbardella altipes*
194 (Henningsmoen, 1948) were compared from three geographic areas: Sardinia (Domusnovas Formation,
195 Italy; Ferretti and Serpagli, 1999) and Normandy (Vaux Limestone, France; Ferretti et al., 2014a) located
196 along the peri-Gondwana margin and Westmorland (Keisley Limestone, UK; Bergström and Ferretti, 2015)
197 located in Avalonia. For a more global assessment of the Late Ordovician conodont faunas, refer to Ferretti
198 et al. (2014b).
199
200 *3.1.1. ESEM and SEM characterization*
201 Conodont elements were preliminarily investigated in order to monitor distribution of major elements.
202 Environmental scanning electron microscopy coupled with microanalyses (SEM/ESEM-EDX) was applied to
203 the entire surface of the conodont specimens, with special attention to detect variations through the
204 element wall thickness. Broken elements were carefully analyzed and scanned for this purpose. Maps of
205 major element (P, Ca, F, C, Cl, K, Na, Ba, Fe, Pb, S) distribution do not vary significantly through the element
206 wall, both for paraconodonts (Fig. 4A) and euconodonts (Fig. 4B). These findings support the presence of
207 the same carbonate-fluoroapatite in the conodont element.
208
209 *3.1.2. μ-XRD measurements and cell parameter refinements*
210 Table SI–1 reports calculated cell parameters for conodonts (Table SI–1a) and non-conodonts (Table SI–
211 1b) listed in Tables 1–2. If analyzed globally, our data enhance an overall considerable dispersion of the cell
212 parameter *a* of the bioapatite. The cell parameter *c*, differently, appears to be highly variable among the

213 euconodonts (Table S1a), and more stable in the other fossil groups, in particular paraconodonts (Table
214 S1a) and brachiopods (Table S1b). Selected data are plotted and discussed in the following sections.
215 Figure 5 plots the bioapatite crystallographic cell parameters *c vs a* for euconodonts and paraconodonts.
216 It is remarkable that paraconodonts and euconodonts clearly occupy two different and non-overlapping
217 fields of the plot. More in detail, the comparison clearly highlights that: i) the cell parameter *a* is smaller in
218 paraconodonts than in euconodonts and it ranges between 9.337(6) and 9.392(6) (Table S1a, specimens
219 A14 and A21, respectively); ii) values of the cell parameter *c* of all paraconodonts are very close to the
220 highest values of *c* of the euconodonts that ranges between 6.857(6) and 6.911(2) (Table S1a, specimens
221 A1 and A89, respectively). Figure 6 plots the bioapatite crystallographic cell parameters *c vs a* for
222 conodonts according to their age, spanning from the late Cambrian (Guzhangian) to the Late Triassic
223 (Carnian). It is highly evident that age does not affect cell parameter distribution. In fact, from a
224 chronological point of view, some values of the cell parameter *a* calculated for the youngest euconodonts
225 (Carboniferous and Triassic) are surprisingly much closer to Cambrian paraconodonts than to Ordovician
226 euconodonts. Figure 7 plots the bioapatite crystallographic cell parameters *c vs a* for selected Late
227 Ordovician conodonts according to their taxonomic assignment (Fig. 7A) and geographic area (Fig. 7B). No
228 correlation is evident in either plots: neither taxonomy (including position occupied within the apparatus
229 architecture) nor geographic location appear to influence cell parameter values.
230
231 *3.2. Other phosphatic fauna (OPF)*
232
233 Phosphatic/phosphatized material was picked exactly from the same residues that had produced the
234 conodont elements that were analyzed, in order to detect additional bioapatite signals and to exclude
235 effects of diverse preparation technique and diagenesis. Well preserved phosphatized ostracodes (Fig. 3G–
236 H, L) and undetermined material (Fig. 3F, K) were picked from the same late Cambrian residue so to offer
237 possible comparison with paraconodonts. A wider age range was covered by the analyzed brachiopods (Fig.
238 3A–C), spanning from the Early Ordovician to the Early Devonian. Particular effort was made to document
239 brachiopods from the three Late Ordovician areas (Sardinia, Normandy and Westmoreland) investigated in

240 detail also with conodonts. Only Late Ordovician bryozoans (Fig. 3D–E), but from three geographic sectors,
241 were processed for investigation. Finally, a few fish teeth (Fig. 3I–J) from Upper Triassic residues were
242 measured. The presence of bioapatite was preliminarily tested by ESEM and SEM techniques so as to
243 exclude non-phosphatic material. No further chemical detailed analysis was attempted.
244
245 *3.2.1. μ-XRD measurements and unit cell parameter refinements*
246 Figure 8 reports bioapatite crystallographic cell parameters for all analyzed OPF. For simplicity, the age-
247 average values of cell parameters calculated for conodonts are reported as well. Main terms of the
248 comparison are: i) values of the cell parameter *a* calculated for all the OPF are generally lower (or, at least,
249 very close) than those calculated for euconodonts, with the exception of a Late Triassic fish tooth
250 (specimen A47; Norian); ii) on the opposite, values of cell parameter *c* calculated for all the OPF are
251 significantly higher (or, at least, very close) than those calculated for euconodonts, with the exception of a
252 Late Ordovician brachiopod (specimen A55; Katian); iii) late Cambrian OPF (ostracodes and undetermined
253 material) share similar values of both cell parameters with paraconodonts, with the exception of an
254 ostracod (specimen A94; Paibian); iv) similar values were calculated also for Early Devonian (Lochkovian)
255 brachiopods and a Late Triassic (Carnian) fish tooth.
256 All results will be further discussed below. However, any conclusion from OPF should be regarded as
257 preliminary since the number of analyzed OPF specimens is significantly lower than conodonts and because
258 we could preliminarily test provenance effects on cell parameters only for bryozoans and brachiopods and
259 age only for brachiopods.
260
261 **4. Discussion**
262
263 Bioapatites are generally classified as francolites [$Ca_5(PO_4, CO_3)_3F$)] or as dahllites [$Ca_5(PO_4, CO_3)_3(OH)$].
264 From a strict mineralogical point of view, these are no longer valid nomenclature forms (discredited by the
265 IMA in 2008) as carbonate is not the dominant species in tetrahedral isomorphic substitutions (type B
266 substitutions) (Wopenka and Pasteris, 2005). Moreover, numerous studies carried out to-date (see Liu et

267 al., 2013 for a review) have shown that many other isomorphic substitutions occur in bioapatites and, in
268 consequence, the chemical formulas of francolite and dahllite cannot be considered completely exhaustive
269 for the composition of these biomaterials. As mentioned in the Introduction, isomorphic substitutions of
270 major elements in apatite significantly affect crystallographic cell parameter dimensions. For example,
271 substitutions of $(CO_3)^{2-}$ for $(PO_4)^{3-}$ results in an increase of the cell parameter *c* and a contraction of the cell
272 parameter *a*, whereas $(CO_3)^{2-}$ for $(OH)^{-}$ substitution produces the opposite results (LeGeros, 1981).
273 Therefore, even if to-date there is no evidence that francolite and dahllite can be considered as the end-
274 members of a continuous solid solution, it is unquestionable that the measurement of cell parameters can
275 provide a nice approximation of major element chemical composition. This approach could be mandatory
276 when both the presence of the C element and small size of the sample prevents a more detailed chemical
277 characterization than semi-quantitative EDS or EDX techniques.

278 Nemliher et al. (2004) combined X-ray diffraction on powdered sample and chemical EDX measurements
279 on fragments of Recent fish and marine mammal skeletons, phosphatic brachiopods and oceanic
280 phosphorites. Data were compared with fossil material and phosphorites of Cretaceous, Miocene and
281 Holocene age. The authors observed a reduction of the cell parameter *a* in fossil material and related this
282 both to the increase of carbonate content and to the decrease in the hydroxyl-ion content subsequent to
283 the recrystallization of apatite. More specifically, they proposed that the substitutions of OH with F are
284 contextual to the progressive decrease in cell volume, evidence that also suggests that these substitutions
285 do not significantly affect cell parameter *c*. Zhang et al. (2017), through a multi-analytical approach
286 combining Raman spectroscopy, high resolution X-ray diffraction and chemical analyses on well-preserved
287 Ordovician coniform conodonts from South China, documented several chemical substitutions occurring
288 during diagenesis that affect conodont tissue types (albid and hyaline crown, and basal body) differently.
289 Such observations were previously highlighted by Trotter et al. (2007) in their examination of hyaline and
290 albid crown tissues using transmission electron microscopy.

291 The absence of significant correlation in our euconodonts between bioapatite cell parameters and
292 taxonomic assignment, age, and geographic provenance of the elements supports the hypothesis that
293 isomorphic substitutions are not exclusively correlated with the age of the fossil. Triassic elements are, in

294 fact, much more deviated compared to the Ordovician ones (Fig. 7). On the other hand, euconodont cell
295 parameters define a higher range of values than paraconodonts (Fig. 5), even if Ordovician euconodonts
296 are closer in age to paraconodonts than to Early Triassic euconodonts. The existence of two clearly
297 separate distribution fields of cell parameters, one for paraconodonts and one for euconodonts, is further
298 strengthened plotting values of bioapatite cell volume (Fig. SI–1). Again, two distinct distributions appear,
299 one for paraconodonts and one for euconodonts. These results improve the knowledge of these elements
300 which were previously studied and distinguished using synchrotron radiation X-ray tomographic microscopy
301 to characterize and compare the microstructure of morphologically similar euconodont and paraconodont
302 elements (Murdock et al., 2013).
303 Transformation of an original bioapatite could also occur by dissolution/recrystallization processes or by
304 metasomatic substitutions. Dissolution/recrystallization drives to the formation of large-size crystals with
305 high crystallinity, whereas metasomatic substitutions normally lead to a reduction of the crystallinity and
306 do not affect crystal size. Notwithstanding which of the two is the main promoter of the transformation,
307 there is general agreement that temperature should favor isomorphic substitution. By restricting the
308 observation to euconodonts, it was thus surprising to find no significant correlation between cell
309 parameters and CAI (Fig. SI–2). Similar conclusions are supported by Zhang et al. (2017) by the analysis of
310 conodonts exhibiting CAI of 1-3, but with no significant relationship between CAI and chemical
311 composition, Raman spectroscopic features, and crystallinity.
312 Comparison of our data and those available in similar studies on conodonts (Fig. SI–3) provides a
313 foremost endorsement of our interpretation. Unfortunately, conodont cell parameters available in the
314 literature are extremely scarce. With the exception of those reported in our previous paper (Ferretti et al.,
315 2017) and here considered, to our knowledge only two researches (Pietzner et al., 1968; Nemliher and
316 Kallaste, 2012) provide this information. Results from Pietzner et al. (1968) were not plotted as information
317 about measurements, and data management are missing. Nemliher and Kallaste (2012) applied an
318 experimental approach, different from ours, but that undoubtedly provides us a useful comparison tool. In
319 fact, the authors calculated cell parameters from X-ray spectra measured on powders produced grinding
320 various specimens of different taxa belonging to different biozones (ranging from the Early Ordovician to

the Silurian). Detected cell parameters could therefore be considered as an average value representative of each biozone. Figure SI–3 shows that there is a nice agreement with our data, including average values calculated for Ordovician elements, and those from the cited authors.

Further support of the absence of a close relationship between cell parameter values and age/geographic provenance is provided by comparing signals of conodonts and other phosphatic fauna (OPF) (Fig. 8). In fact, excluding the out of range cell parameter values above mentioned among OPF (specimens A47 and A55), remaining data could be better sorted considering the fossil group rather than its age or locality.

Lack of additional material does not allow definitive conclusions to be formulated without speculation. However, if our preliminary data are confirmed by further measurements on larger and more varied faunal collections, including also Recent material and with diverse preservation (Ferretti et al., 2012), it appears that primary biomineralization provides an indelible footprint, only mediated by fossilization and diagenetic processes.

5. Conclusions

This research has added to routine morphological and chemical qualitative characterization, achievable through optical and electronic microscopy, by integrating a crystallographic approach based on X-ray microdiffraction (μ-XRD) to gain enhanced structural information about conodonts and other bioapatite fossils. Microdiffraction measurements, recently introduced in conodont studies by our research group, is, in fact, a powerful tool for obtaining crystallographic information when dealing with small-sized samples like conodont elements. Moreover, μ-XRD is a non-destructive technique for dealing with irreplaceable material. The methodological approach and the results here obtained were additionally strengthened by comparison with data from the literature that had been obtained through conventional methods (X-ray powder diffraction) that parallel our findings.

As reported in the literature, bioapatite crystallographic cell parameters strongly depend on different isomorphic substitutions. Our data reveal that cell parameters calculated for paraconodonts significantly

differ from those derived for euconodonts. In fact, paraconodonts bear smaller cell parameters *a* and higher cell parameters *c*, very close to the highest values of *c* of euconodonts. Moreover, cell parameters calculated for both paraconodonts and euconodonts appear to be independent of age, taxonomic assignment, geographic provenance and, for euconodonts, CAI (i.e., temperature). Other phosphatic/phosphatized material from the same residues producing conodonts are characterized by values of the cell parameters that, in a preliminary way, appear to be mainly correlated with the type of organism even if, for some of them, a correlation also with age cannot be completely ruled out.

It is, therefore, conceivable that major element content strongly depends not only on fossilization, diagenesis and metasomatism, but mostly on the primary bioapatite composition. In other words, from a close crystal-chemical point of view, it is not possible to unequivocally conclude, for example, that the cell parameter *a*, smaller in paraconodonts than in euconodonts, is the direct consequence of a sort of "francolitization" process (i.e., the formation, for progressive and successive isomorphic substitutions, of the end-member francolite that, as already pointed out, was never proved) during fossilization and/or diagenesis.

Acknowledgements

A long list of friends provided us conodont material and taxonomic assignment of the specimens. Enrico Serpagli created, over the course of his superb career, an invaluable conodont collection at the University of Modena and Reggio Emilia for future studies. Claudia Spalletta, Maria Cristina Perri, Michele Mazza, Manuel Rigo and Carlo Corradini are greatly acknowledged for their invaluable support. We are especially grateful to Massimo Tonelli (University of Modena and Reggio Emilia – Scientific Instruments Facility) for SEM/ESEM expertise.

The Editor-in-Chief, Thomas J. Algeo, the Guest Editors, Alyssa Bancroft and John Repetski, and two anonymous reviewers provided valuable comments during the course of this study. Financial support was provided under grant FAR 2016 PAsTIME, University of Modena and Reggio Emilia. This paper is a contribution to IGCP Project 653 “The onset of the Great Ordovician Biodiversity Event”.

References

Banfield J.F., Zhang H., 2001. Nanoparticles in the environment. Rev. Mineral. Geochem. 44(1), 1–58.

Bergström, S.M., Ferretti, A., 2015. Conodonts in the Upper Ordovician Keisley Limestone of northern England: taxonomy, biostratigraphical significance and biogeographical relationships. Pap. Palaeont. 93, 1–32.

Boskey, A., 2007. Mineralization of bones and teeth. Elements 3, 385–391.

Cazalbou, S., Combes, C., Eichert, D., Rey, C., 2004. Adaptive physico-chemistry of bio-related calcium phosphates. J. Mater. Chem. 14, 2148–2153.

Chlupáč, I., Kříž, J., Schönlaub, H.P., 1980. Field Trip E, ECOS II, Barrandian. Abh. Geol. Bundesanst. 35, 147–180.

Cohen, K.M., Finney, S.C., Gibbard, P.L., Fan, J.-X., 2013; updated 2018. The ICS international chronostratigraphic chart. Episodes 36, 199–204.

Farabegoli, E., Perri, M.C., 1998. Scythian and Anisian conodonts from the Sotto le Rive section (Southern Alps, Italy). Giorn. Geol. 60, 254–259.

Ferretti, A., Bergström, S.M., Barnes, C.R., 2014b. Katian (Upper Ordovician) conodonts from Wales. Palaeontology 57(4), 801–831.

Ferretti, A., Cavalazzi, B., Barbieri, R., Westall, F., Foucher, F., Todesco, R., 2012. From black-and-white to colour in the Silurian. Palaeogeogr., Palaeoclimatol., Palaeoecol. 367–368, 505–519.

Ferretti, A., Malferrari, D., Medici, L., Savioli, M., 2017. Diagenesis does not invent anything new: Precise replication of conodont structures by secondary apatite. Sci. Rep. 7 (1), 1624–1632.

Ferretti, A., Messori, A., Bergström, S.M., 2014a. Composition and significance of the Katian (Upper Ordovician) conodont fauna of the Vaux Limestone (“Calcaire des Vaux”) in Normandy, France. Est. J. Earth Sci. 63(4), 214–219.

Ferretti, A., Serpagli, E., 1999. Late Ordovician conodont faunas from southern Sardinia, Italy: biostratigraphic and paleogeographic implications. Boll. Soc. Paleont. Ital. 37(2–3), 215–236.

Glimcher, M.J., 2006. Bone: Nature of the calcium phosphate crystals and cellular, structural, and physical chemical mechanisms in their formation. Rev. Mineral. Geochem. 64. 223–282.

Holland, T.J.B., Redfern, S.A.T., 1997. Unit cell refinement from powder diffraction data: the use of regression diagnostics. Mineral. Mag. 61, 65–77.

Holmden, C., Creaser, R.A., Muehlenbachs, K., Bergström, S.M., Leslie, S.A., 1996. Isotopic and elemental systematics of Sr and Nd in 454 Ma biogenic apatites: implications for paleoseawater studies. Earth. Planet. Sci. Lett. 142, 425–437.

Hughes, J.M., Cameron, M., Crowley, K.D., 1989. Structural variations in natural F, OH, and Cl apatites. Am. Mineral. 74, 870–876.

Hughes, J.M., Rakovan, J., 2002. The Crystal Structure of Apatite, Ca5(PO4)3(F,OH,Cl). Rev. Mineral. Geochem. 48. 1– 12.

Kallaste, T., Nemliher, J., 2005. Apatite varieties in extant and fossil vertebrate mineralized tissues. J. Appl. Cryst. 38, 587–594.

Keenan, S.W., 2016. From bone to fossil: A review of the diagenesis of bioapatite. Am. Mineral. 101(9), 1943–1951.

Kohn, M.J., Schoeninger, M.J., Barker, W.W., 1999. Altered states: effects of diagenesis on fossil tooth chemistry. Geochim. Cosmochim. Acta 63(18), 2737–2747.

Kovaçs, S., Papsova, J., Perri, M.C., 1996. New Middle Triassic conodonts of the *Gondolella szabòi-G. trammeri* lineage from the West Carpathian Mts and from the Southern Alps. Acta Geol. Hung. 39(1), 101–128.

LeGeros, R.Z., 1981. Apatites in biological systems. Prog. Cryst. Growth Charact. Mater. 4(1–2), 1–45.

LeGeros, R.Z., LeGeros, J.P., 1984. Phosphate minerals in human tissue. In: Nriagu, J.O., Moore, P.B. (Eds.), Phosphate Minerals. Springer-Verlag, New York, pp. 351–395.

Liu, Q., Huang, S., Pekka Matinlinna, J., Chen, Z., Pan, H., 2013. Insight into Biological Apatite: Physiochemical Properties and Preparation Approaches. BioMed. Research International 929, 7–48.

Mann, S., 2001. Biomineralization: Principles and Concepts in Bioinorganic Materials Chemistry. Oxford University Press, Oxford, pp. 1–198.

427 Martínez-Pérez, C., Rayfield, E.J., Purnell, M.A., Donoghue, P.C.J., 2014. Finite element, occlusal, microwear
428 and microstructural analyses indicate that conodont microstructure is adapted to dental function.
429 Palaeontology 57(5), 1059–1066.
430 Mazza, M., Martínez-Pérez, C. 2015. Unravelling conodont (Conodonta) ontogenetic processes in the Late
431 Triassic through growth series reconstructions and X-ray microtomography. Boll. Soc. Paleont. Ital. 54(3),
432 161–186.
433 Mazza, M., Rigo, M., Gullo, M., 2012. Taxonomy and stratigraphic record of the Upper Triassic conodonts of
434 the Pizzo Mondello section (Western Sicily, Italy), GSSP candidate for the base of the Norian. Riv. It.
435 Paleont. Strat. 118(1), 85–130.
436 McConnell, D., 1973. Apatite – its crystal chemistry, mineralogy, utilization and geological and biological
437 occurrences. Applied Mineralogy, Springer-Verlag, Wien, pp. 1–111.
438 Müller, K.J., Hinz, I. 1991. Upper Cambrian conodonts from Sweden. Fossils & Strata 28, 1–153.
439 Murdock, D.J.E., Dong, X.-P., Repetski, J.E., Marone, F., Stampanoni, M., Donoghue, P.C.J., 2013. The origin
440 of conodonts and of vertebrate mineralized skeletons. Nature 502, 546–549.
441 Nemliher, J.G., Baturin, G.N., Kallaste, T.E., Murdmaa, I.O., 2004. Transformation of Hydroxyapatite of Bone
442 Phosphate from the Ocean Bottom during Fossilization. Lithol. Miner. Resour. 39(5), 468–479.
443 Nemliher, J., Kallaste, T., 2012. Conodont bioapatite resembles vertebrate enamel by XRD properties. Est. J.
444 Earth Sci. 61(3), 191–192.
445 Pasteris, J.D., Wopenka, B., Valsami-Jones, E., 2008. Bone and tooth mineralization: why apatite? Elements
446 4(2), 97–104.
447 Perri, M.C., Andraghetti, M., 1987. Permian–Triassic boundary and Early Triassic conodonts from the
448 Southern Alps, Italy. Riv. It. Paleont. Strat. 93 (3), 291–328.
449 Perri, M.C., Spalletta, C., 1998. Latest Devonian and Early Carboniferous conodonts from the Casera
450 Collinetta di Sotto A section (Carnic Alps, Italy). Giorn. Geol. 60, 168–181.
451 Pietzner, H., Vahl, J., Werner, H., Ziegler, W., 1968. Zur chemischen Zuzammensetzung und
452 Mikromorphologie der Conodonten. Palaeontographica 128, 115–152.

453 Rodríguez-Lorenzo, L.M., Hart, J.N., Gross, K.A., 2003. Structural and Chemical Analysis of Well-Crystallized
454 Hydroxyfluorapatites. J. Phys. Chem. B 107, 8316–8320.
455 Skinner, H.C.W., 2005. Biominerals. Mineral. Mag. 69, 621–641.
456 Spalletta, C., Perri, M.C., 1998a. The Frasnian-Famennian boundary at the Pramosio A section (Carnic Alps,
457 Italy). Giorn. Geol. 60, 198–205.
458 Spalletta, C., Perri, M.C., 1998b. Lower Carboniferous conodonts at the Tournaisian/Visean boundary in the
459 Dolina section (Carnic Alps, Italy). Giorn. Geol. 60, 244–253.
460 Szaniawski, H., 1971. New species of Upper Cambrian conodonts from Poland. Acta Palaeontol. Pol. XVI(4),
461 401–413.
462 Trotter, J.A., Eggins, S.M., 2006. Chemical systematics of conodont apatite determined by laser ablation
463 ICPMS. Chem. Geol. 233(3), 196–216.
464 Trotter, J.A., Fitz Gerald, J.D., Kokkonen, H., Barnes, C.R., 2007. New insights into the ultrastructure,
465 permeability, and integrity of conodont apatite determined by transmission electron microscopy.
466 Lethaia 40(2), 97–110.
467 Trotter, J.A., Korsch, M.J., Nicoll, R.S., Whitford, D.J., 1999. Sr isotopic variation in single conodont
468 elements: implications for defining the Sr seawater curve. Boll. Soc. Paleont. Ital. 37(2–3), 507–514.
469 Trueman, C.N., Tuross, N., 2002. Trace elements of recent and fossil bone apatite. Rev. Mineral. Geochem.
470 48, 489–521.
471 Viira, V. 1970. Conodonts of the Varangu Member (Estonian Upper Tremadoc). Eesti NSV Tead. Akad. Toim.
472 Keemia Geol. 19, 224–233.
473 Wenzel, B., Lécuyer, C., Joachimski, M.M., 2000. Comparing oxygen isotope records of Silurian calcite and
474 phosphate–$\delta^{18}O$ compositions of brachiopods and conodonts. Geochim. Cosmochim. Acta 64(11), 1859–
475 1872.
476 Wopenka, B., Pasteris, J.D., 2005. A mineralogical perspective on the apatite in bone. Mater. Sci. Eng. C 25,
477 131–143.

Zhang, L., Cao, L., Zhao, L., Algeo, T.J., Chen, Z.Q., Li, Z., Lv, Z., Wang, X., 2017. Raman spectral, elemental, crystallinity, and oxygen-isotope variations in conodont apatite during diagenesis. Geochim. Cosmochim. Acta 210(1), 184–207.

CAPTION TO FIGURES

Fig. 1. Different time frames investigated in this study plotted on the latest version of the International Commission on Stratigraphy Chronostratigraphic Chart (2018/08: http://www.stratigraphy.org/index.php/ics-chart-timescale; see Cohen et al., 2013, updated 2018).

Fig. 2. Some of the conodont elements analyzed in this study. A: *Westergaardodina* sp., late Cambrian, specimen no. A11, IPUM 29101, Västergötland (Sweden); B: *Furnishina alata* Szaniawski, 1971, late Cambrian, specimen no. A18, IPUM 29102, Żarnowiec (Poland); C: *Furnishina* sp., late Cambrian, specimen no. A14, IPUM 29103, Västergötland (Sweden); D: *Paltodus deltifer deltifer* (Lindström, 1955), Early Ordovician, specimen no. A6, IPUM 29104, Öland (Sweden); E: *Hamarodus brevirameus* (Walliser, 1964), M element, Late Ordovician, specimen no. 82, IPUM 29105, Normandy (France); F: *Amorphognathus* sp., Pb element, Late Ordovician, specimen no. A41, IPUM 29106, Sardinia (Italy); G: *Amorphognathus* sp., Pb element, Late Ordovician, specimen no. A27, IPUM 29107, Westmorland (UK); H: *Lanea omoalpha* (Murphy and Valenzuela-Ríos, 1999), Early Devonian, specimen no. A2, IPUM 29108, U Topolů (Bohemia); I: *Rhipidognathus symmetricus* Branson, Mehl and Branson, 1951, Late Ordovician, specimen no. A22, IPUM 29109, Saluda Dolomite (USA); J: *Scabbardella altipes* (Henningsmoen, 1948), Late Ordovician, specimen no. 45, IPUM 29110, Normandy (France); K: *Amorphognathus* sp., Pa element, Late Ordovician, specimen no. A98, IPUM 29111, Westmorland (UK); L: *Zieglerodina planilingua* (Murphy and Valenzuela-Ríos, 1999), Early Devonian, specimen no. A1, IPUM 29112, U Topolů (Bohemia); M: *Polygnathus decorosus* Stauffer, 1938, Late Devonian, specimen no. A83, IPUM 29113, Carnic Alps (Italy); N: *Palmatolepis* sp., Late Devonian, specimen no. A82, IPUM 29114, Carnic Alps (Italy); O: *Gnathodus* sp., Middle Mississippian, specimen no. A78, IPUM 29115, Carnic Alps (Italy); P: *Branmehla werneri* (Ziegler, 1957), Late Devonian,

specimen no. A81, IPUM 29116, Carnic Alps (Italy); Q: *Palmatolepis triangularis* Sannemann, 1955, Late Devonian, specimen no. A101, IPUM 29117, Texas (USA); R: *Palmatolepis subperlobata* Branson and Mehl, 1934, Late Devonian, specimen no. A102, IPUM 29118, Texas (USA); S, U: *Pachycladina obliqua* Staesche, 1964, Early Triassic, specimens no. A87 and A86, IPUM 29119 and IPUM 29121, Dolomites (Italy); T: unrecognizable fragment, Early Mississippian, specimen no. A77, IPUM 29120, Carnic Alps (Italy); V: unrecognizable fragment, Middle Triassic, specimen no. A84, IPUM 29122, Dolomites (Italy); W–X: *Carnepigondolella pseudodiebeli* (Kozur, 1972), Late Triassic, specimens no. A44 and A43, IPUM 29123 and IPUM 29124, Sicily (Italy).

Scale bars correspond to 200 µm.

Fig. 3. Some of the other phosphatic fauna analyzed in this study. A–C: brachiopods, Early Devonian (A) and Late Ordovician (B–C), specimens no. A3, A26 and A36, IPUM 29125–29127, U Topolů (Bohemia), Westmorland (UK) and Sardinia (Italy), respectively; D–E: bryozoans, Late Ordovician, specimens no. A24 and A61, IPUM 29128 and IPUM 29129, Saluda Dolomite (USA) and Normandy (France), respectively; F, K: undetermined phosphatic material, late Cambrian, specimens no. A95 and A96, IPUM 29130 and IPUM 29135, Västergötland (Sweden); G–H, L: ostracodes, late Cambrian, specimens no. A17, A94 and A93, IPUM 29131, IPUM 29132 and IPUM 29136, Västergötland (Sweden); I–J: fish teeth, Late Triassic, specimens no. A45 and A46, IPUM 29133 and IPUM 29134, Sicily (Italy).

Scale bars correspond to 500 µm except for G (400 µm) and H, L (300 µm).

Fig. 4. Chemical composition. ESEM image and SEM-EDS elemental maps (P, Ca, F, C, and Cl). A: *Furnishina* sp., late Cambrian, specimen no. A110, IPUM 29137, Västergötland (Sweden). B: *Scabbardella altipes* (Henningsmoen, 1948), Late Ordovician; specimen no. A109, IPUM 29138, Normandy (France).

Scale bars correspond to 200 µm.

Fig. 5. Binary plot of bioapatite crystallographic unit-cell parameters *c vs a* for euconodonts and paraconodonts.

Fig. 6. Binary plot of bioapatite crystallographic unit-cell parameters *c vs a* of conodonts by age.

Fig. 7. Binary plot of bioapatite crystallographic unit-cell parameters *c vs a* of Late Ordovician conodonts by taxonomy (A) and geographic provenance (B).

Fig. 8. Binary plot of bioapatite crystallographic unit-cell parameters *c vs a* for other phosphatic/phosphatized fauna (ostracodes, brachiopods, bryozoans and fish teeth) compared with average values of conodonts by age.

CAPTION TO TABLES

Table 1. Conodont taxa analyzed in the present paper, referred to geographic location/formation, age, and most relevant literature. P: paraconodont; E: euconodont.

Table 2. Other phosphatic/phosphatized taxa analyzed in the present paper, referred to geographic location and age.

INTERNATIONAL CHRONOSTRATIGRAPHIC CHART

IUGS www.stratigraphy.org International Commission on Stratigraphy v 2018/08

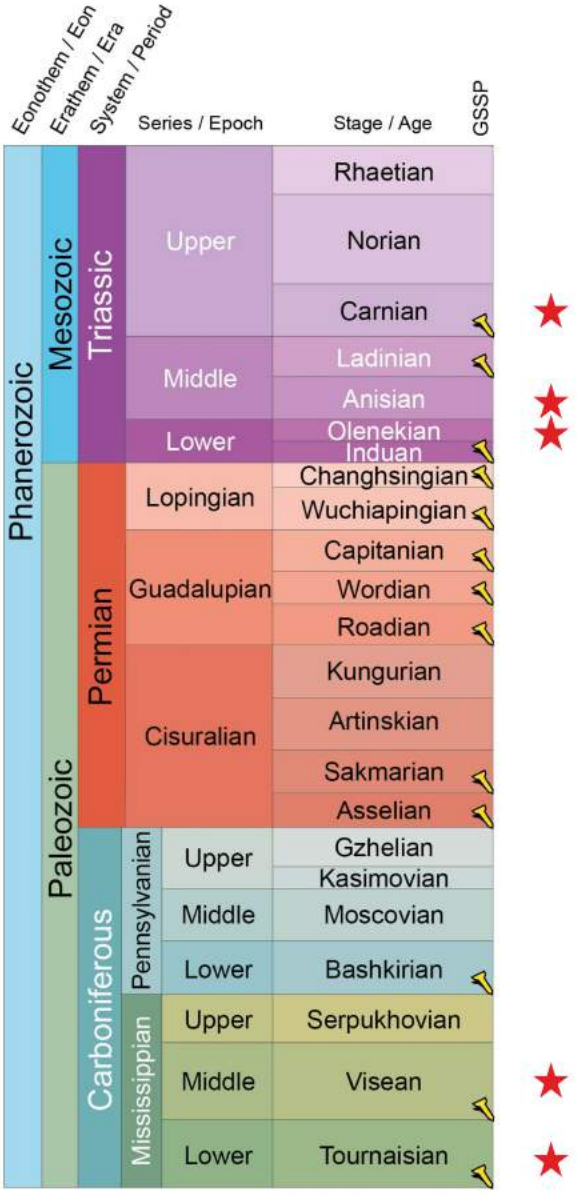

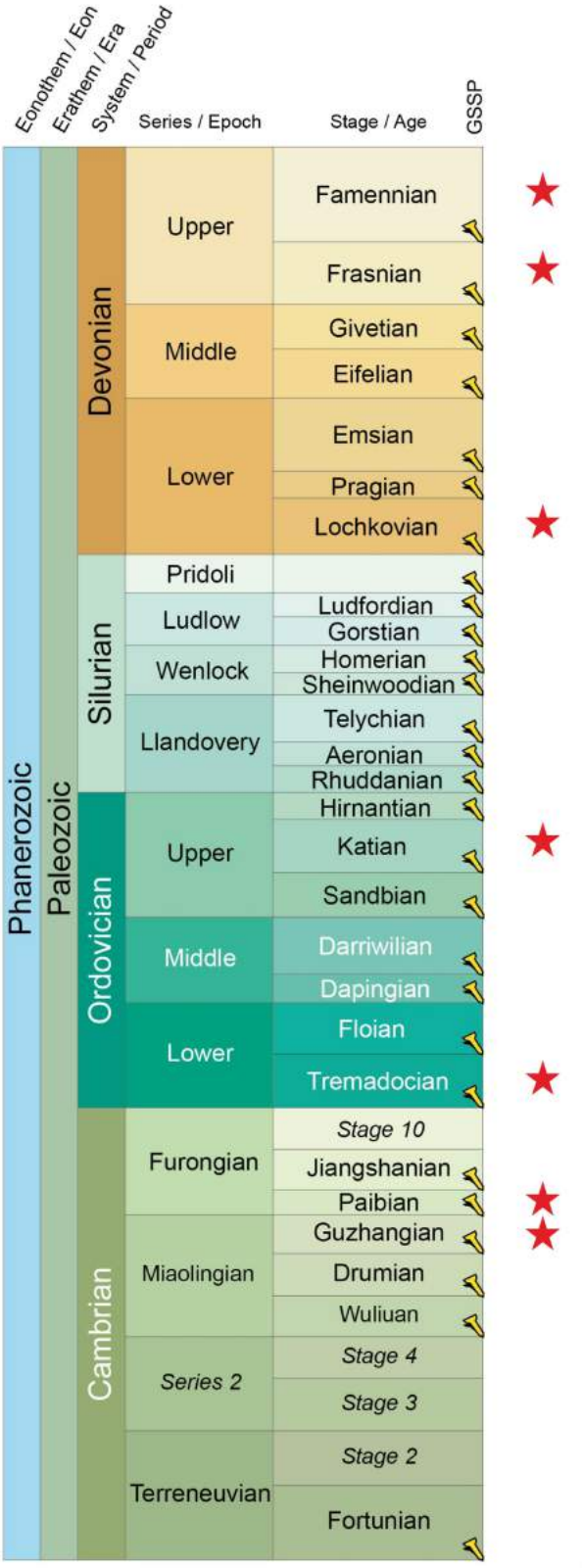

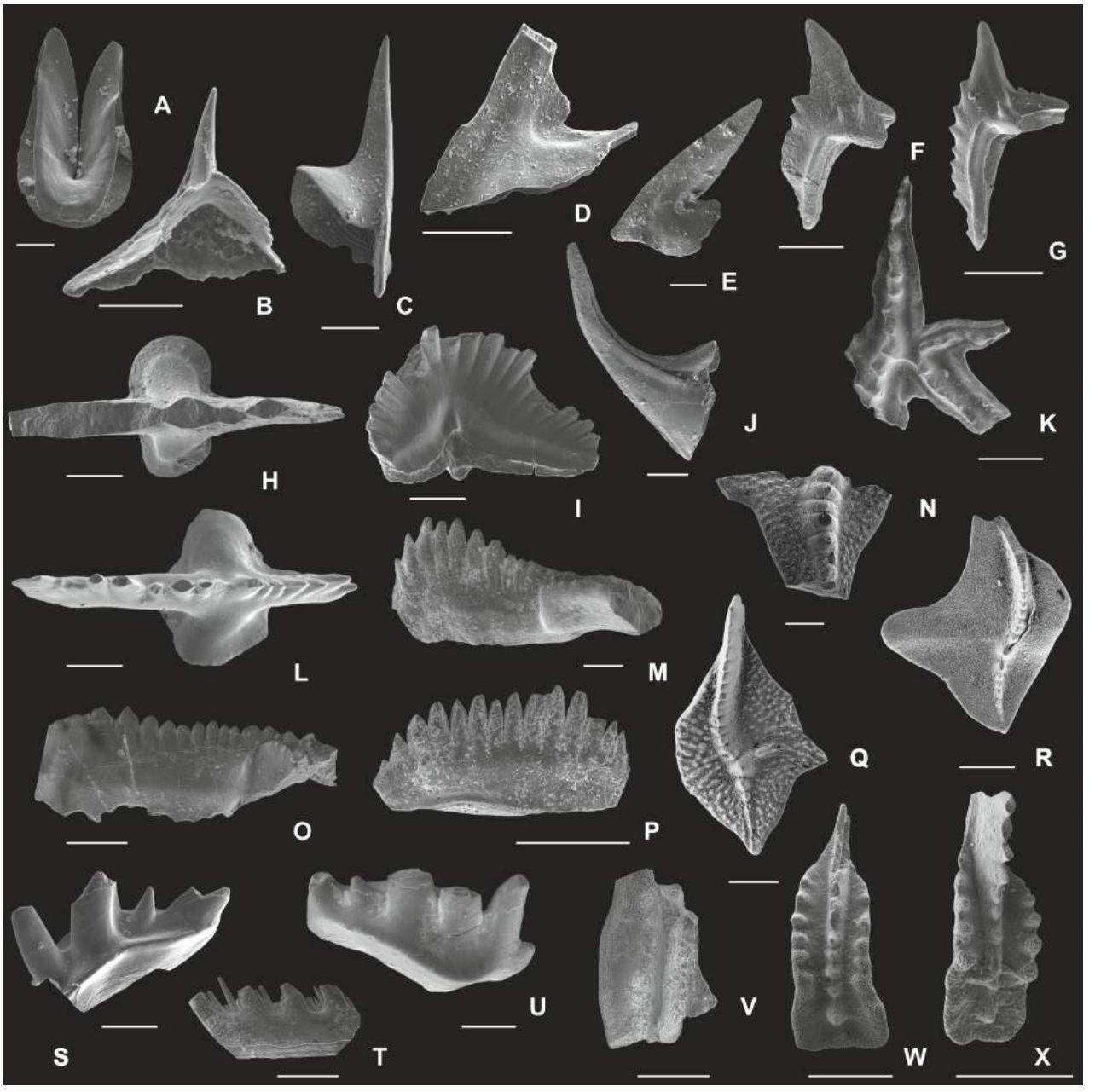
A
B
C
D
E
F
G
H
I
J
K
L
M
N
O
P
Q
R
S
T
U
V
W
X

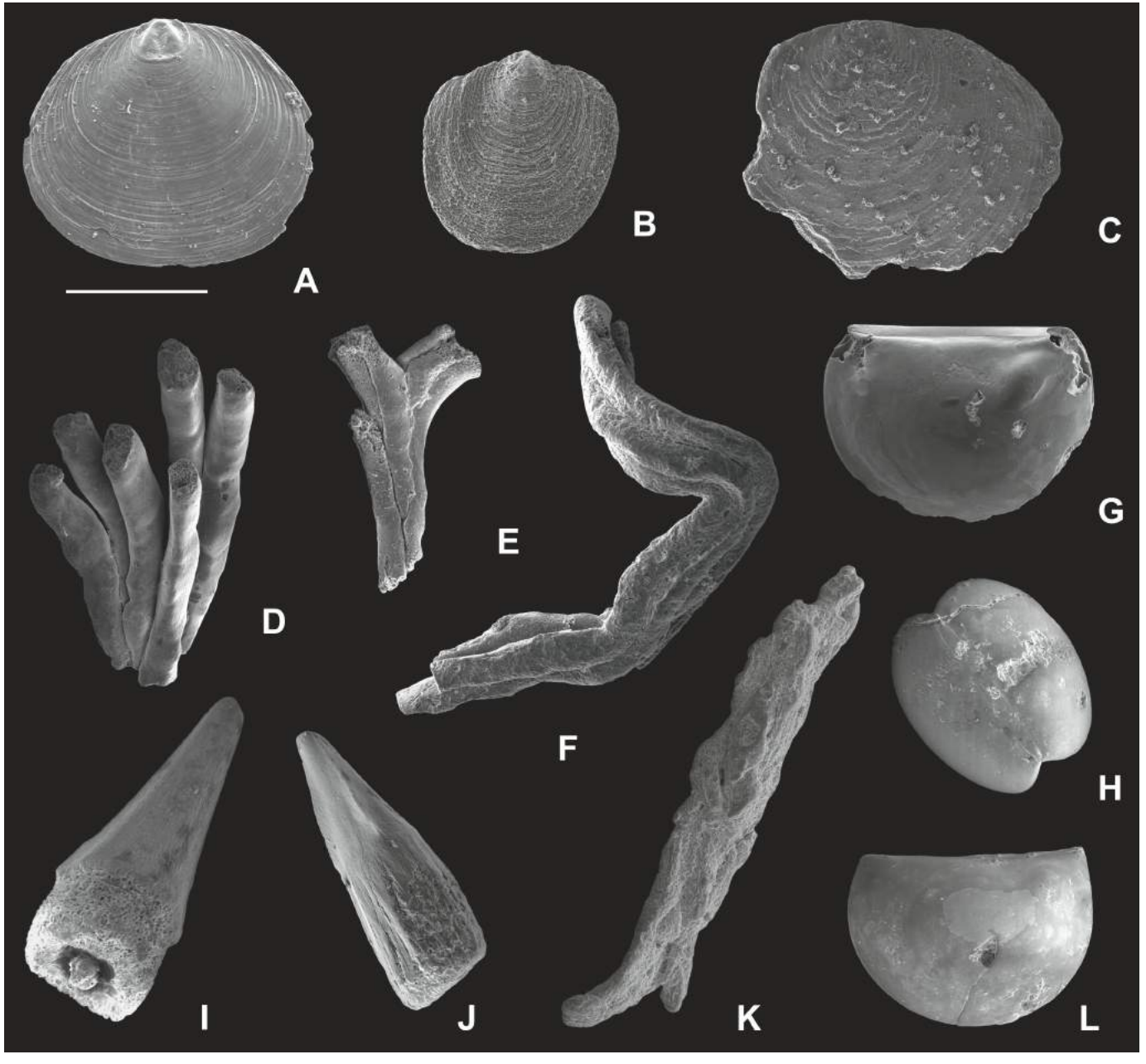
A
B
C
D
E
F
G
H
I
J
K
L

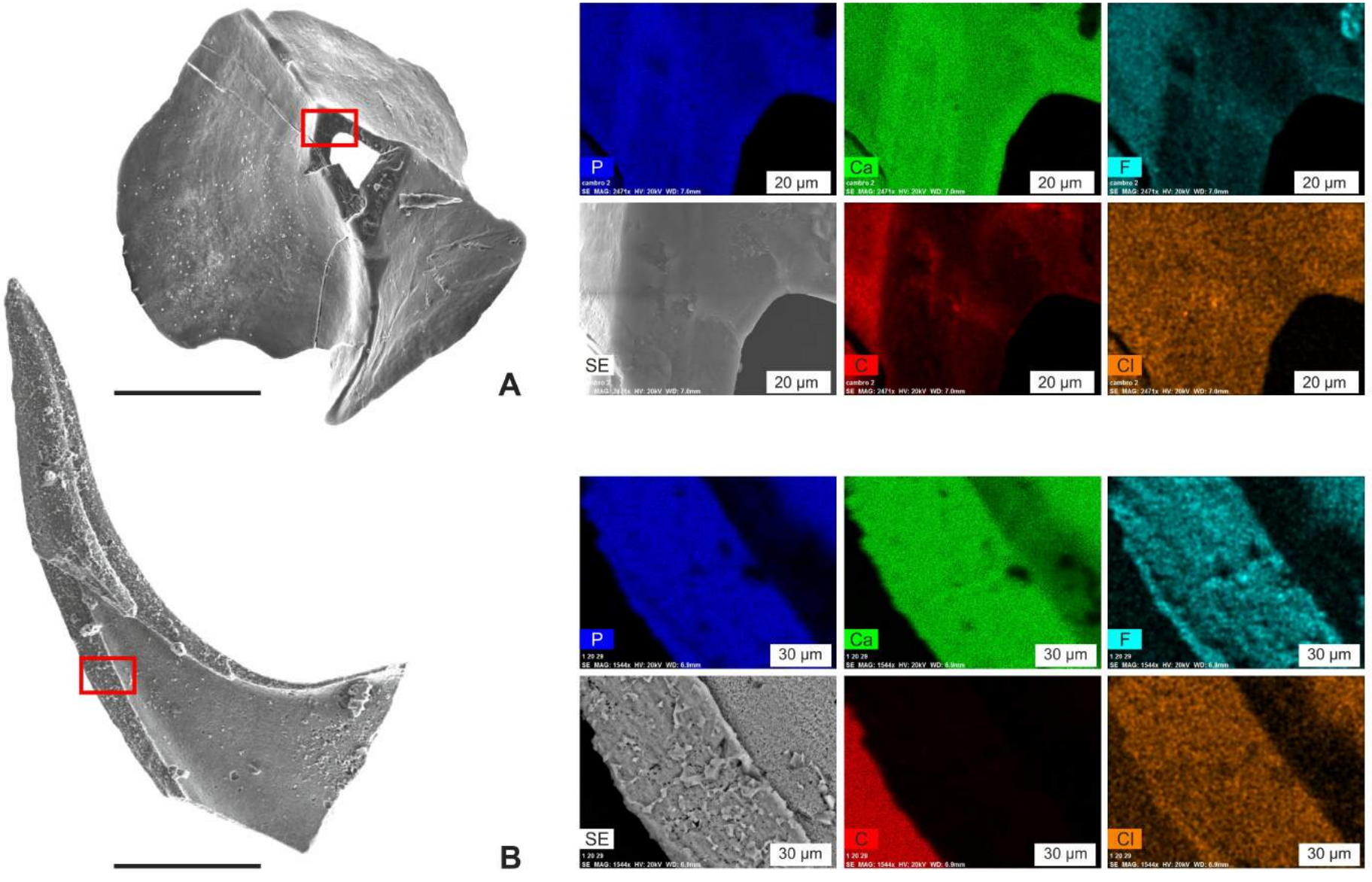
A
B
P
Ca
F
SE
C
Cl
20 µm
30 µm

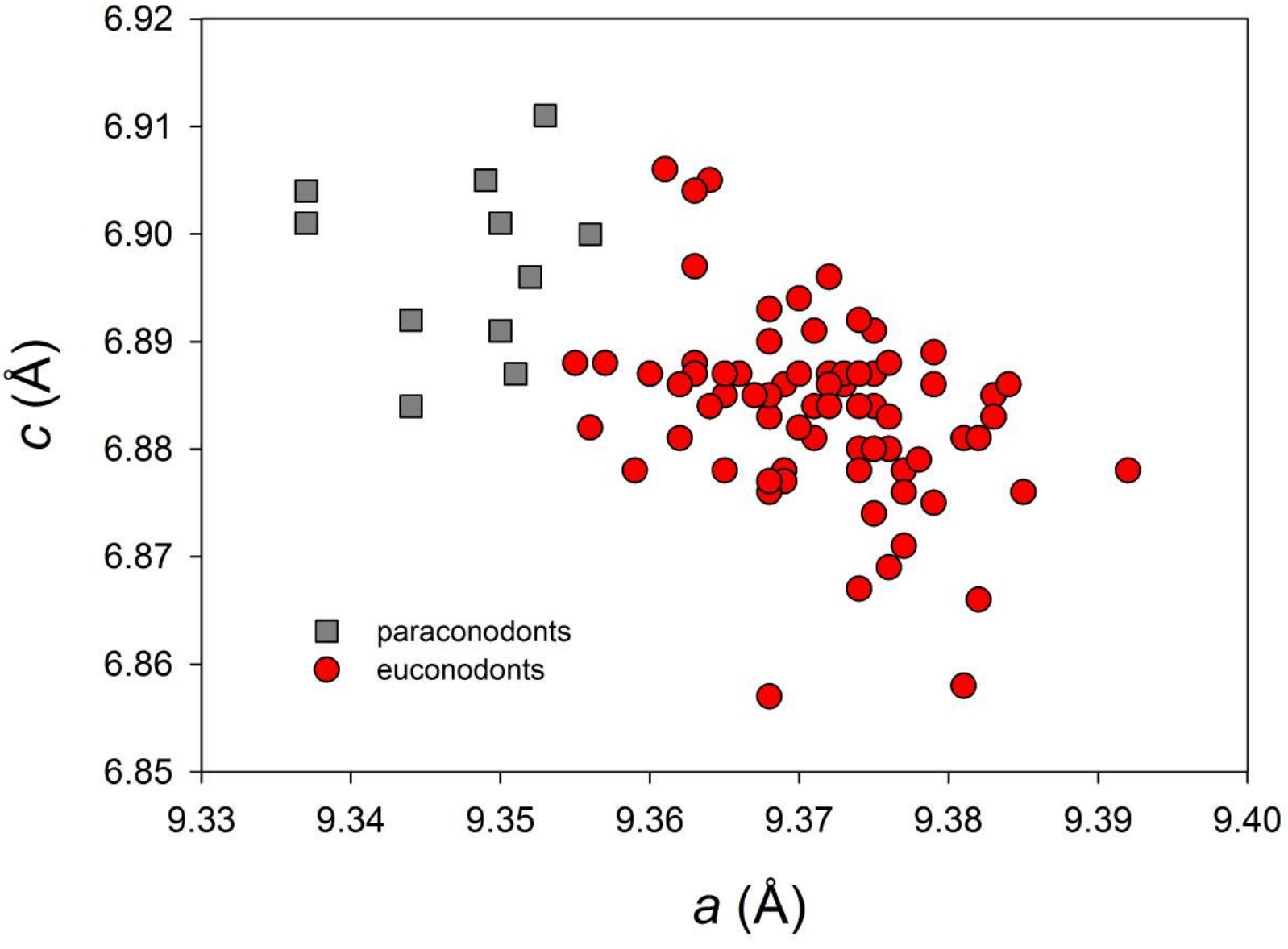
6.92
6.91
6.90
6.89
6.88
6.87
6.86
6.85
c (Å)
9.33
9.34
9.35
9.36
9.37
9.38
9.39
9.40
a (Å)
paraconodonts
euconodonts

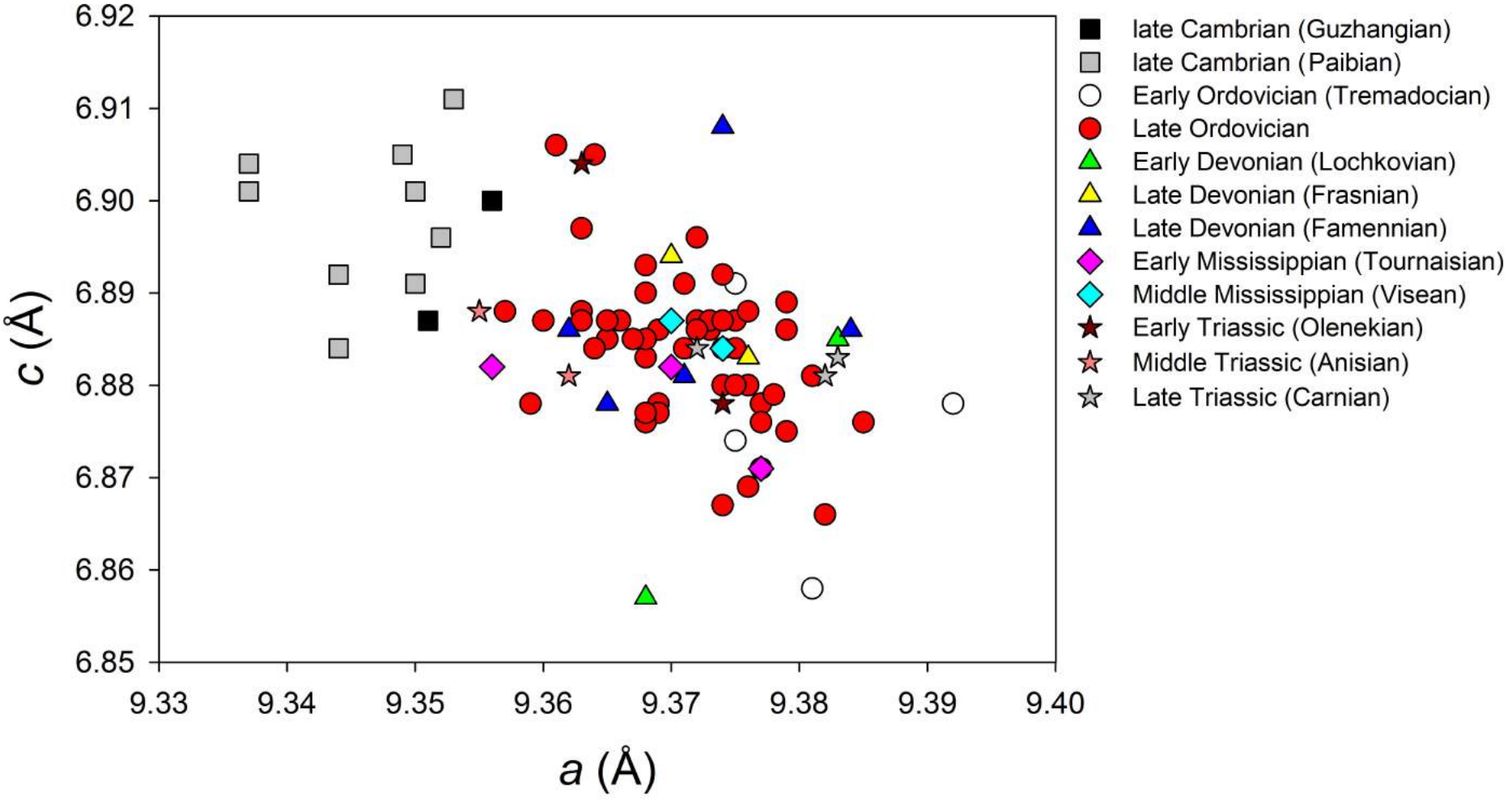
6.92
6.91
6.90
6.89
6.88
6.87
6.86
6.85
c (Å)
9.33
9.34
9.35
9.36
9.37
9.38
9.39
9.40
a (Å)
late Cambrian (Guzhangian)
late Cambrian (Paibian)
Early Ordovician (Tremadocian)
Late Ordovician
Early Devonian (Lochkovian)
Late Devonian (Frasnian)
Late Devonian (Famennian)
Early Mississippian (Tournaisian)
Middle Mississippian (Visean)
Early Triassic (Olenekian)
Middle Triassic (Anisian)
Late Triassic (Carnian)

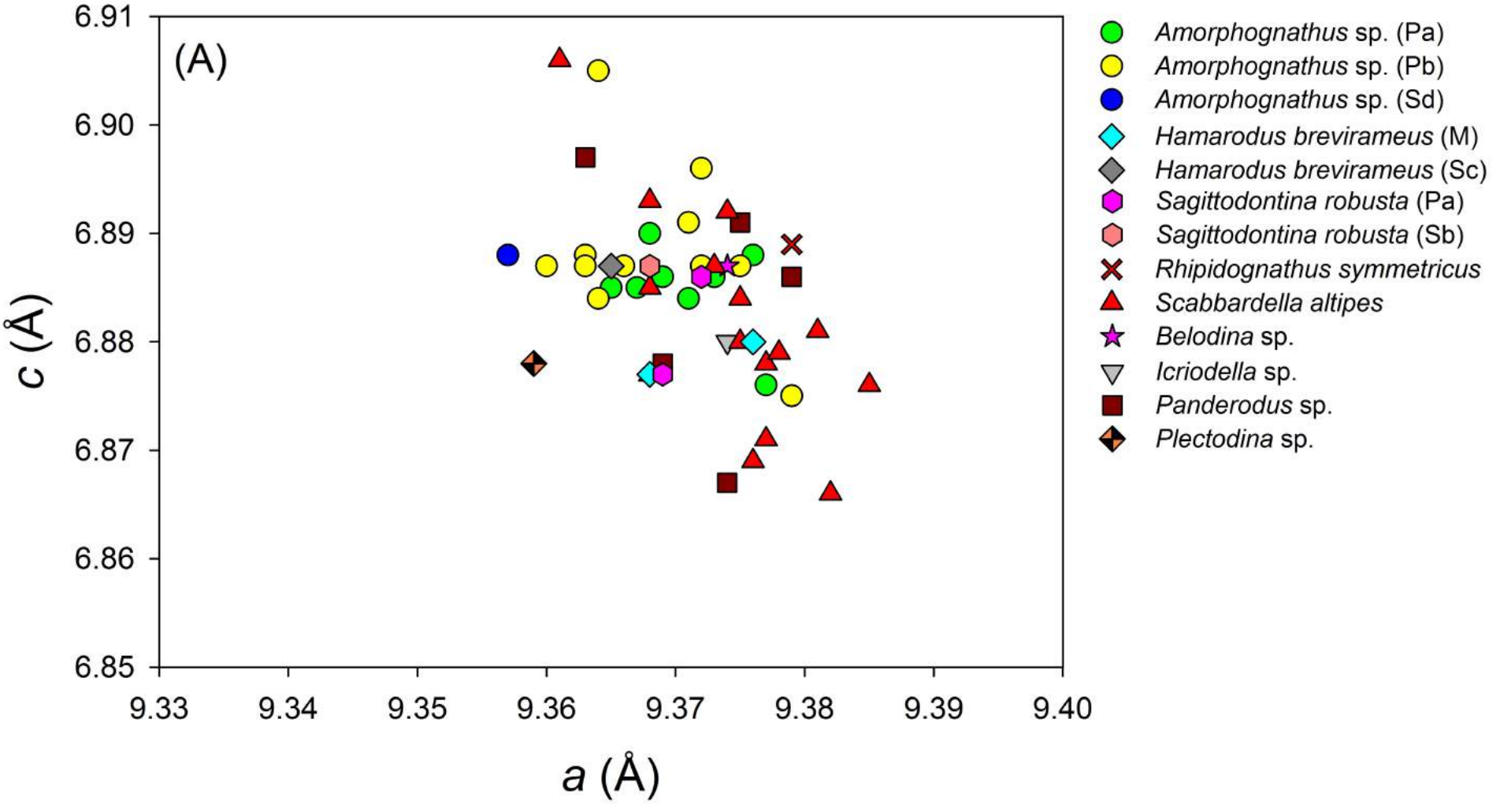
(A)
6.91
6.90
6.89
6.88
6.87
6.86
6.85
c (Å)
9.33
9.34
9.35
9.36
9.37
9.38
9.39
9.40
a (Å)
Amorphognathus sp. (Pa)
Amorphognathus sp. (Pb)
Amorphognathus sp. (Sd)
Hamarodus brevirameus (M)
Hamarodus brevirameus (Sc)
Sagittodontina robusta (Pa)
Sagittodontina robusta (Sb)
Rhipidognathus symmetricus
Scabbardella altipes
Belodina sp.
Icriodella sp.
Panderodus sp.
Plectodina sp.

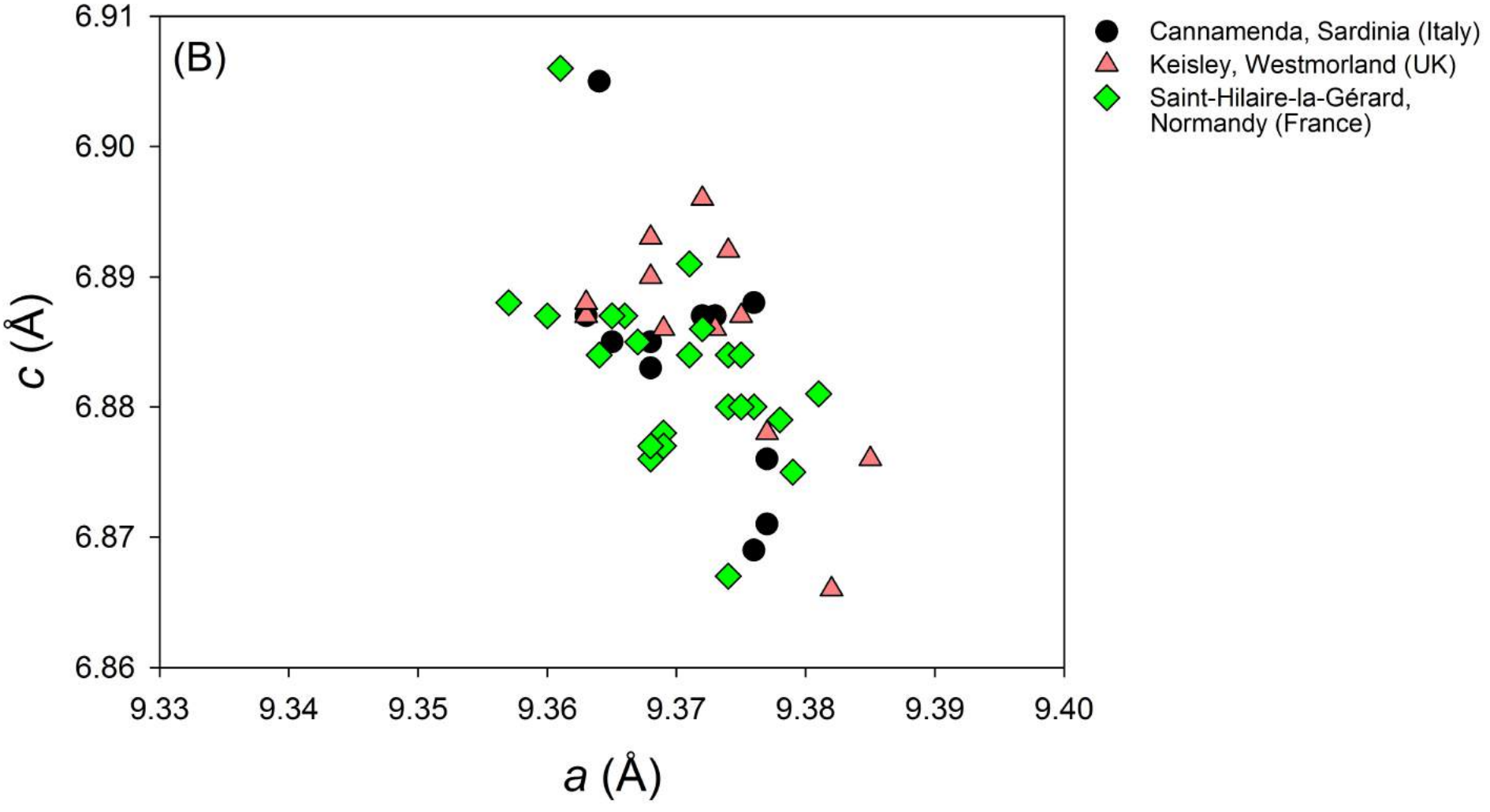
(B)
6.91
6.90
6.89
6.88
6.87
6.86
c (Å)
9.33
9.34
9.35
9.36
9.37
9.38
9.39
9.40
a (Å)
Cannamenda, Sardinia (Italy)
Keisley, Westmorland (UK)
Saint-Hilaire-la-Gérard, Normandy (France)

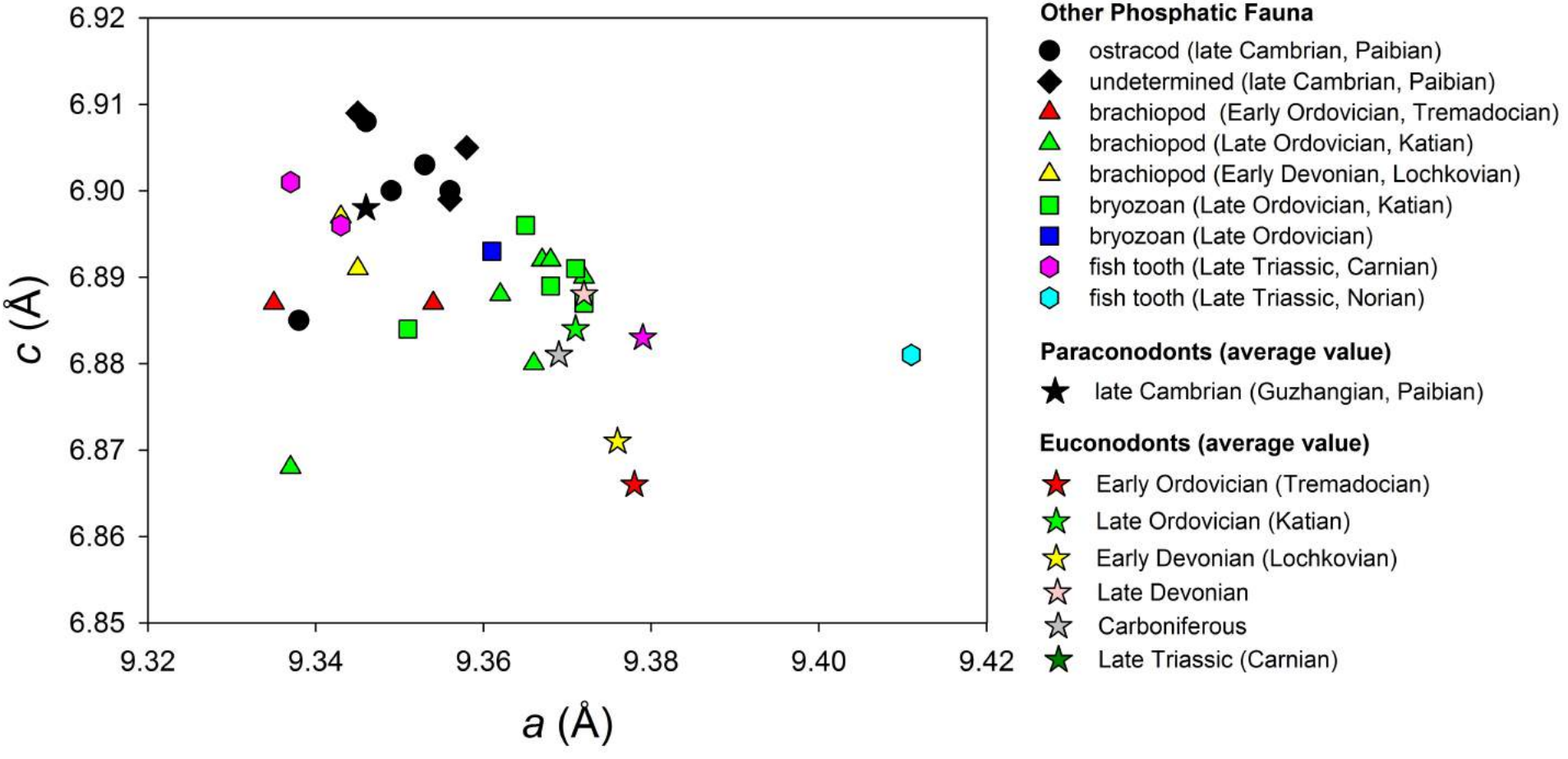
6.92
6.91
6.90
6.89
6.88
6.87
6.86
6.85
c (Å)
9.32
9.34
9.36
9.38
9.40
9.42
a (Å)
Other Phosphatic Fauna
ostracod (late Cambrian, Paibian)
undetermined (late Cambrian, Paibian)
brachiopod (Early Ordovician, Tremadocian)
brachiopod (Late Ordovician, Katian)
brachiopod (Early Devonian, Lochkovian)
bryozoan (Late Ordovician, Katian)
bryozoan (Late Ordovician)
fish tooth (Late Triassic, Carnian)
fish tooth (Late Triassic, Norian)
Paraconodonts (average value)
late Cambrian (Guzhangian, Paibian)
Euconodonts (average value)
Early Ordovician (Tremadocian)
Late Ordovician (Katian)
Early Devonian (Lochkovian)
Late Devonian
Carboniferous
Late Triassic (Carnian)

Code	n° elements	Conodont taxa	Locality/Formation	Age	P/E	CAI	reference paper(s)/ collection
A18-A19	2	*Furnishina alata* Szaniawski, 1971	Żarnowiec (Poland)	Cambrian Miaolingian (Guzhangian)	P		Szaniawski, 1971
A11-A12, A90-A91	4	*Westergaardodina* sp.	Kinnekulle, Västergötland (Sweden)	Cambrian Furongian (Paibian)	P		Müller and Hinz, 1991
A13-A14, A88-A89, A110	4	*Furnishina* sp.	Kinnekulle, Västergötland (Sweden)	Cambrian Furongian (Paibian)	P		Müller and Hinz, 1991
A15	1	unrecognizable fragment	Kinnekulle, Västergötland (Sweden)	Cambrian Furongian (Paibian)	P		Müller and Hinz, 1991
A5-A6	2	*Paltodus deltifer deltifer* (Lindström, 1955)	Öland (Sweden)	Early Ordovician (Tremadocian)	E	1.5	IPUM Collection
A10	1	unrecognizable fragment	Öland (Sweden)	Early Ordovician (Tremadocian)	E	1.5	IPUM Collection
A20-A21	2	*Paltodus deltifer pristinus* (Viira, 1970)	Northern Estonia	Early Ordovician (Tremadocian)	E	1.5	Viira, 1970
A30-A31, A98-A99	4	*Amorphognathus* sp. (Pa)	Keisley, Westmorland (UK)	Late Ordovician (Katian)	E	4	Bergström and Ferretti, 2015
A27-A29	3	*Amorphognathus* sp. (Pb)	Keisley, Westmorland (UK)	Late Ordovician (Katian)	E	4	Bergström and Ferretti, 2015
A32-A34, A74-A75	5	*Scabbardella altipes* (Henningsmoen, 1948)	Keisley, Westmorland (UK)	Late Ordovician (Katian)	E	4	Bergström and Ferretti, 2015
A38, A66-A67	3	*Amorphognathus* sp. (Pa)	Cannamenda, Sardinia (Italy)	Late Ordovician (Katian)	E	5	Ferretti and Serpagli, 1999
A37, A41, A68, A72	4	*Amorphognathus* sp. (Pb)	Cannamenda, Sardinia (Italy)	Late Ordovician (Katian)	E	5	Ferretti and Serpagli, 1999
A39-A40, A69-A70	4	*Scabbardella altipes* (Henningsmoen, 1948)	Cannamenda, Sardinia (Italy)	Late Ordovician (Katian)	E	5	Ferretti and Serpagli, 1999
A49-A51	3	*Amorphognathus* sp. (Pa)	Saint-Hilaire-la-Gérard, Normandy (France)	Late Ordovician (Katian)	E	4-5	Ferretti et al., 2014a
62, A52, A107-A108	4	*Amorphognathus* sp. (Pb)	Saint-Hilaire-la-Gérard, Normandy (France)	Late Ordovician (Katian)	E	4-5	Ferretti et al., 2014a
17	1	*Amorphognathus* sp. (Sd)	Saint-Hilaire-la-Gérard,	Late Ordovician (Katian)	E	4-5	Ferretti et al., 2014a

			Normandy (France)				
68, 82	2	*Hamarodus brevirameus* (Walliser, 1964) (M)	Saint-Hilaire-la-Gérard, Normandy (France)	Late Ordovician (Katian)	E	4-5	Ferretti et al., 2014a
49	1	*Hamarodus brevirameus* (Walliser, 1964) (Sc)	Saint-Hilaire-la-Gérard, Normandy (France)	Late Ordovician (Katian)	E	4-5	Ferretti et al., 2014a
21	1	*Icriodella* sp.	Saint-Hilaire-la-Gérard, Normandy (France)	Late Ordovician (Katian)	E	4-5	Ferretti et al., 2014a
20, 56, A53	3	*Panderodus* sp.	Saint-Hilaire-la-Gérard, Normandy (France)	Late Ordovician (Katian)	E	4-5	Ferretti et al., 2014a
24, 41	2	*Sagittodontina robusta* Knüpfer, 1967 (Pa)	Saint-Hilaire-la-Gérard, Normandy (France)	Late Ordovician (Katian)	E	4-5	Ferretti et al., 2014a
46	1	*Sagittodontina robusta* Knüpfer, 1967 (Sd)	Saint-Hilaire-la-Gérard, Normandy (France)	Late Ordovician (Katian)	E	4-5	Ferretti et al., 2014a
45, 59-60, 91, 103, A54, A109	6	*Scabbardella altipes* (Henningsmoen, 1948)	Saint-Hilaire-la-Gérard, Normandy (France)	Late Ordovician (Katian)	E	4-5	Ferretti et al., 2014a
A22	1	*Rhipidognathus symmetricus* Branson, Mehl and Branson, 1951	Saluda Dolomite (USA)	Late Ordovician	E	1	IPUM Collection
A23	1	*Panderodus* sp.	Saluda Dolomite (USA)	Late Ordovician	E	1	IPUM Collection
A104	1	*Belodina* sp.	Kimmswick Formation, Missouri (USA)	Late Ordovician	E	1	IPUM Collection
A105	1	*Plectodina* sp.	Kimmswick Formation, Missouri (USA)	Late Ordovician	E	1	IPUM Collection
A106	1	*Panderodus* sp.	Kimmswick Formation, Missouri (USA)	Late Ordovician	E	1	IPUM Collection
A1	1	*Zieglerodina planilingua* (Murphy and Valenzuela-Ríos, 1999)	U Topolů (Bohemia)	Early Devonian (Lochkovian)	E	3	Chlupáč et al., 1980
A2	1	*Lanea omoalpha* (Murphy and Valenzuela-Ríos, 1999)	U Topolů (Bohemia)	Early Devonian (Lochkovian)	E	3	Chlupáč et al., 1980
A82	1	*Palmatolepis* sp.	Pramosio A, Carnic Alps (Italy)	Late Devonian (Frasnian)	E	4.5	Spalletta and Perri, 1998a
A83	1	*Polygnathus decorosus* Stauffer, 1938	Pramosio A, Carnic Alps (Italy)	Late Devonian (Frasnian)	E	4.5	Spalletta and Perri, 1998a
A80	1	unrecognizable fragment	Casera Collinetta di Sotto A, Carnic Alps (Italy)	Late Devonian (Famennian)	E	4.5	Perri and Spalletta, 1998

A81	1	*Branmehla werneri* (Ziegler, 1957)	Casera Collinetta di Sotto A, Carnic Alps (Italy)	Late Devonian (Famennian)	E	4.5	Perri and Spalletta, 1998
A101	1	*Palmatolepis triangularis* Sannemann, 1955	Texas (USA)	Late Devonian (Famennian)	E	2	IPUM Collection
A102	1	*Palmatolepis subperlobata* Branson and Mehl, 1934	Texas (USA)	Late Devonian (Famennian)	E	2	IPUM Collection
A103	1	*Icriodus* sp.	Texas (USA)	Late Devonian (Famennian)	E	2	IPUM Collection
A76-A77, A100	3	unrecognizable fragments	Dolina, Carnic Alps (Italy)	Carboniferous Early Mississippian (Tournaisian)	E	4.5	Spalletta and Perri, 1998b
A78-A79	2	*Gnathodus* sp.	Dolina, Carnic Alps (Italy)	Carboniferous Middle Mississippian (Visean)	E	4-4.5	Spalletta and Perri, 1998b
A86-A87	2	*Pachycladina obliqua* Staesche, 1964	Cencenighe Galleria, Dolomites (Italy)	Early Triassic (Olenekian)	E	5.5-6	Perri and Andraghetti, 1987
A84-A85	2	unrecognizable fragments	Sotto le Rive, Dolomites (Italy)	Middle Triassic (Anisian)	E	1.5	Kovaçs et al., 1996; Farabegoli and Perri, 1998
A42-A44	3	*Carnepigondolella pseudodiebeli* (Kozur, 1972)	Pizzo Mondello, Sicani Mountains, Sicily (Italy)	Late Triassic (Carnian)	E	1.5	Mazza et al., 2012; Mazza and Martínez-Pérez, 2015

Code	Faunal element	Locality	Age
A16	ostracod	Kinnekulle, Västergötland (Sweden)	Cambrian Furongian (Paibian)
A17	ostracod	Kinnekulle, Västergötland (Sweden)	Cambrian Furongian (Paibian)
A92	ostracod	Kinnekulle, Västergötland (Sweden)	Cambrian Furongian (Paibian)
A93	ostracod	Kinnekulle, Västergötland (Sweden)	Cambrian Furongian (Paibian)
A94	ostracod	Kinnekulle, Västergötland (Sweden)	Cambrian Furongian (Paibian)
A95	undetermined	Kinnekulle, Västergötland (Sweden)	Cambrian Furongian (Paibian)
A96	undetermined	Kinnekulle, Västergötland (Sweden)	Cambrian Furongian (Paibian)
A97	undetermined	Kinnekulle, Västergötland (Sweden)	Cambrian Furongian (Paibian)
A7	brachiopod	Öland (Sweden)	Early Ordovician (Tremadocian)
A8	brachiopod	Öland (Sweden)	Early Ordovician (Tremadocian)
A9	brachiopod	Öland (Sweden)	Early Ordovician (Tremadocian)
A25	brachiopod	Keisley, Westmorland (UK)	Late Ordovician (Katian)
A26	brachiopod	Keisley, Westmorland (UK)	Late Ordovician (Katian)
A73	brachiopod	Cannamenda, Sardinia (Italy)	Late Ordovician (Katian)
A36	brachiopod	Cannamenda, Sardinia (Italy)	Late Ordovician (Katian)
A55	brachiopod	Saint-Hilaire-la-Gérard, Normandy (France)	Late Ordovician (Katian)
A64	brachiopod	Saint-Hilaire-la-Gérard, Normandy (France)	Late Ordovician (Katian)
A3	brachiopod	U Topolů (Bohemia)	Early Devonian (Lochkovian)
A4	brachiopod	U Topolů (Bohemia)	Early Devonian (Lochkovian)
A35	bryozoan	Cannamenda, Sardinia (Italy)	Late Ordovician (Katian)
A71	bryozoan	Cannamenda, Sardinia (Italy)	Late Ordovician (Katian)
A58	bryozoan	Saint-Hilaire-la-Gérard, Normandy (France)	Late Ordovician (Katian)
A61	bryozoan	Saint-Hilaire-la-Gérard, Normandy (France)	Late Ordovician (Katian)
A65	bryozoan	Saint-Hilaire-la-Gérard, Normandy (France)	Late Ordovician (Katian)
A24	bryozoan	Saluda Dolomite (USA)	Late Ordovician
A45	fish tooth	Pizzo Mondello, Sicani Mountains, Sicily (Italy)	Late Triassic (Carnian)
A46	fish tooth	Pizzo Mondello, Sicani Mountains, Sicily (Italy)	Late Triassic (Carnian)
A47	fish tooth	Pizzo Mondello, Sicani Mountains, Sicily (Italy)	Late Triassic (Norian)

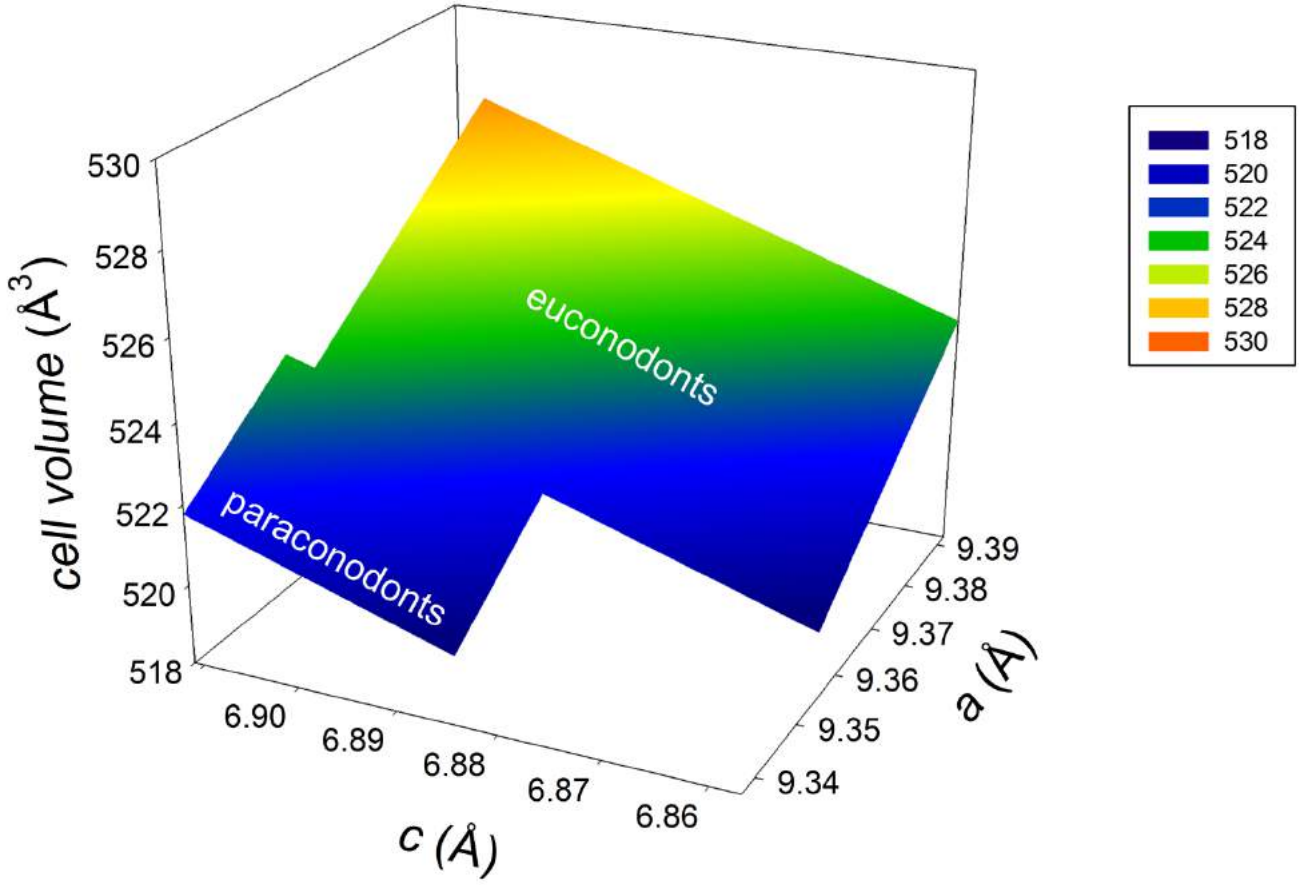

Figure SI-1. Bioapatite cell volume distribution surface calculated for paraconodonts and euconodonts.

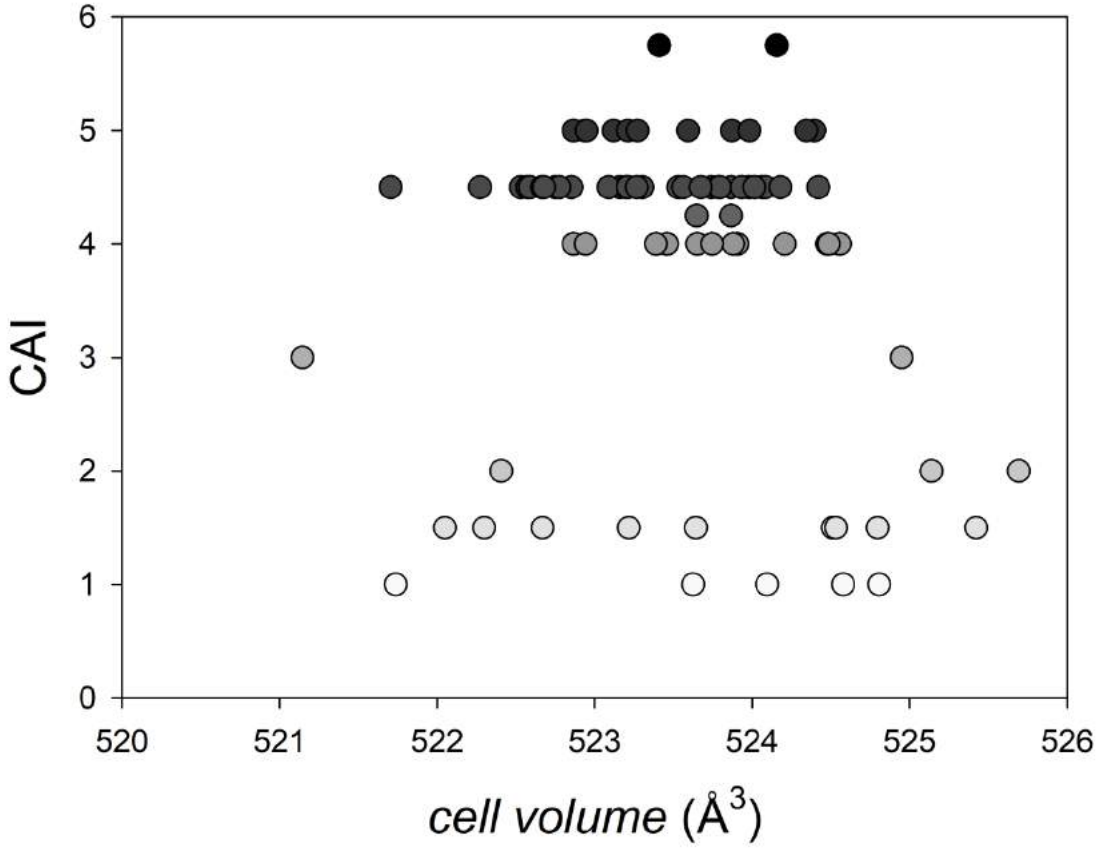

Figure SI-2. Distribution of bioapatite cell volumes calculated for euconodonts in function of the CAI. Grey tones are used exclusively to facilitate reading (light grey, low CAI; dark grey, high CAI).

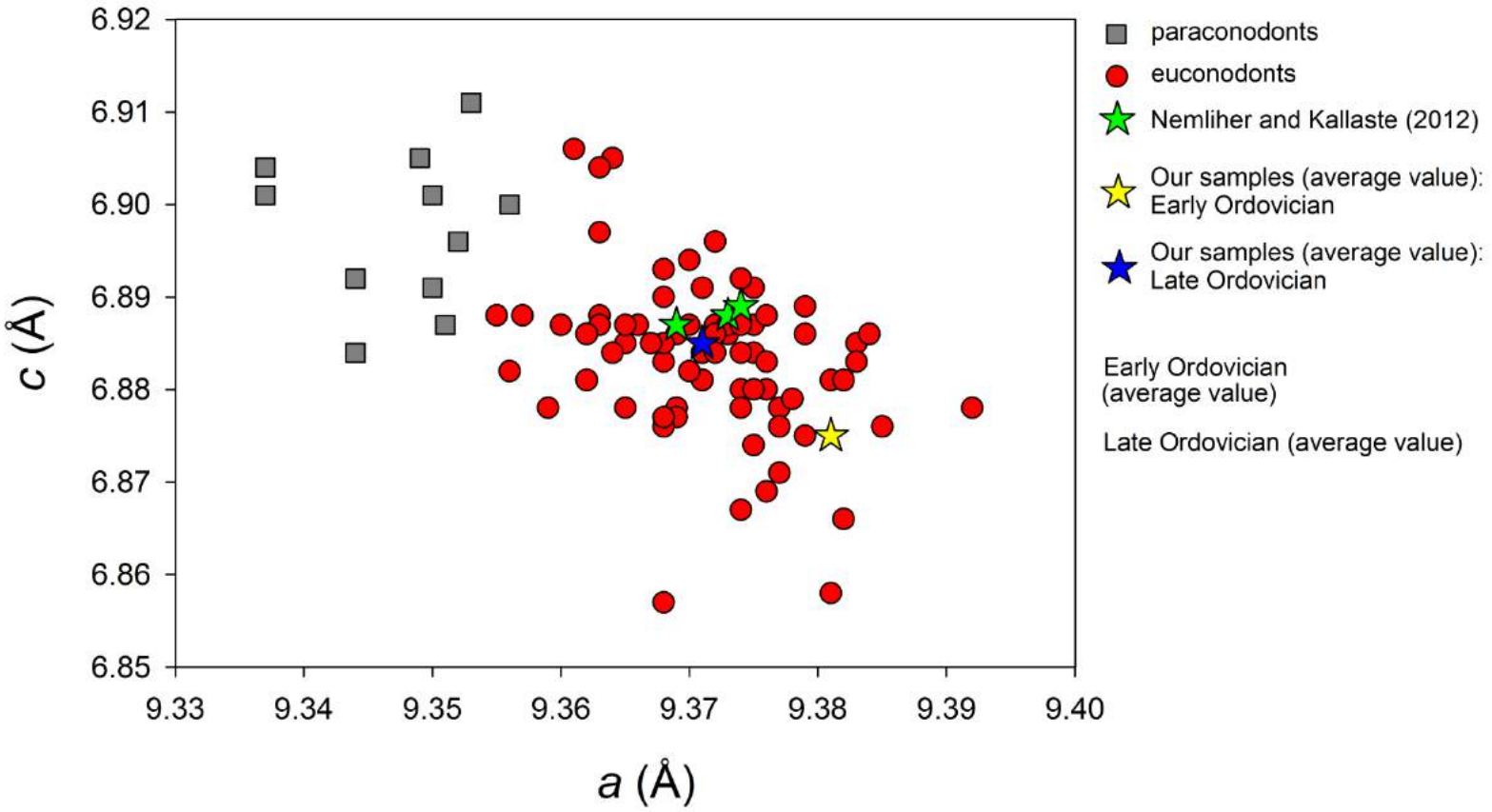

Figure SI-3. Binary plot of bioapatite unit-cell parameters *c vs a* for our euconodonts and paraconodonts compared with literature data.

Table SI-1a. Bioapatite cell parameters calculated for conodonts. For additional details, see Table 1. P: paraconodont; E: euconodont.

Code	*a* (Å)	*c* (Å)	Taxa	Locality/Formation	Age	P / E	CAI
A18	9.356(6)	6.900(4)	*Furnishina alata* Szaniawski, 1971	Żarnowiec (Poland)	Cambrian Miaolingian (Guzhangian)	P	
A19	9.351(4)	6.887(4)	*Furnishina alata* Szaniawski, 1971	Żarnowiec (Poland)	Cambrian Miaolingian (Guzhangian)	P	
A11	9.344(4)	6.892(4)	*Westergaardodina* sp.	Kinnekulle, Västergötland (Sweden)	Cambrian Furongian (Paibian)	P	
A12	9.344(3)	6.884(3)	*Westergaardodina* sp.	Kinnekulle, Västergötland (Sweden)	Cambrian Furongian (Paibian)	P	
A90	9.350(4)	6.891(3)	*Westergaardodina* sp.	Kinnekulle, Västergötland (Sweden)	Cambrian Furongian (Paibian)	P	
A91	9.352(4)	6.896(4)	*Westergaardodina* sp.	Kinnekulle, Västergötland (Sweden)	Cambrian Furongian (Paibian)	P	
A13	9.349(2)	6.905(2)	*Furnishina* sp.	Kinnekulle, Västergötland (Sweden)	Cambrian Furongian (Paibian)	P	
A14	9.337(6)	6.901(5)	*Furnishina* sp.	Kinnekulle, Västergötland (Sweden)	Cambrian Furongian (Paibian)	P	
A88	9.350(3)	6.901(5)	*Furnishina* sp.	Kinnekulle, Västergötland (Sweden)	Cambrian Furongian (Paibian)	P	
A89	9.353(2)	6.911(2)	*Furnishina* sp.	Kinnekulle, Västergötland (Sweden)	Cambrian Furongian (Paibian)	P	
A15	9.337(3)	6.904(2)	unrecognizable fragment	Kinnekulle, Västergötland (Sweden)	Cambrian Furongian (Paibian)	P	
A5	9.375(3)	6.874(5)	*Paltodus deltifer deltifer* (Lindström, 1955)	Öland (Sweden)	Early Ordovician (Tremadocian)	E	1.5
A6	9.381(2)	6.858(6)	*Paltodus deltifer deltifer* (Lindström, 1955)	Öland (Sweden)	Early Ordovician (Tremadocian)	E	1.5

A20	9.375(2)	6.891(4)	*Paltodus deltifer deltifer* (Lindström, 1955)	Northern Estonia	Early Ordovician (Tremadocian)	E	1.5
A21	9.392(6)	6.878(6)	*Paltodus deltifer deltifer* (Lindström, 1955)	Northern Estonia	Early Ordovician (Tremadocian)	E	1.5
A30	9.363(2)	6.887(3)	*Amorphognathus* sp. (Pa)	Keisley, Westmorland (UK)	Late Ordovician (Katian)	E	4
A31	9.368(5)	6.890(3)	*Amorphognathus* sp. (Pa)	Keisley, Westmorland (UK)	Late Ordovician (Katian)	E	4
A98	9.369(2)	6.886(4)	*Amorphognathus* sp. (Pa)	Keisley, Westmorland (UK)	Late Ordovician (Katian)	E	4
A99	9.373(3)	6.886(4)	*Amorphognathus* sp. (Pa)	Keisley, Westmorland (UK)	Late Ordovician (Katian)	E	4
A27	9.375(2)	6.887(3)	*Amorphognathus* sp. (Pb)	Keisley, Westmorland (UK)	Late Ordovician (Katian)	E	4
A28	9.372(2)	6.896(2)	*Amorphognathus* sp. (Pb)	Keisley, Westmorland (UK)	Late Ordovician (Katian)	E	4
A29	9.363(3)	6.888(6)	*Amorphognathus* sp. (Pb)	Keisley, Westmorland (UK)	Late Ordovician (Katian)	E	4
A32	9.382(3)	6.866(6)	*Scabbardella altipes* (Henningsmoen, 1948)	Keisley, Westmorland (UK)	Late Ordovician (Katian)	E	4
A33	9.374(3)	6.892(5)	*Scabbardella altipes* (Henningsmoen, 1948)	Keisley, Westmorland (UK)	Late Ordovician (Katian)	E	4
A34	9.368(2)	6.893(4)	*Scabbardella altipes* (Henningsmoen, 1948)	Keisley, Westmorland (UK)	Late Ordovician (Katian)	E	4
A74	9.385(4)	6.876(5)	*Scabbardella altipes* (Henningsmoen, 1948)	Keisley, Westmorland (UK)	Late Ordovician (Katian)	E	4
A75	9.377(2)	6.878(4)	*Scabbardella altipes* (Henningsmoen, 1948)	Keisley, Westmorland (UK)	Late Ordovician (Katian)	E	4
A38	9.365(3)	6.885(2)	*Amorphognathus* sp. (Pa)	Cannamenda, Sardinia (Italy)	Late Ordovician (Katian)	E	5
A66	9.377(2)	6.876(3)	*Amorphognathus* sp. (Pa)	Cannamenda, Sardinia (Italy)	Late Ordovician (Katian)	E	5

A67	9.376(2)	6.888(3)	*Amorphognathus* sp. (Pa)	Cannamenda, Sardinia (Italy)	Late Ordovician (Katian)	E	5
A37	9.363(3)	6.887(4)	*Amorphognathus* sp. (Pb)	Cannamenda, Sardinia (Italy)	Late Ordovician (Katian)	E	5
A41	9.364(2)	6.905(3)	*Amorphognathus* sp. (Pb)	Cannamenda, Sardinia (Italy)	Late Ordovician (Katian)	E	5
A68	9.368(3)	6.883(4)	*Amorphognathus* sp. (Pb)	Cannamenda, Sardinia (Italy)	Late Ordovician (Katian)	E	5
A72	9.372(3)	6.887(6)	*Amorphognathus* sp. (Pb)	Cannamenda, Sardinia (Italy)	Late Ordovician (Katian)	E	5
A39	9.377(2)	6.871(6)	*Scabbardella altipes* (Henningsmoen, 1948)	Cannamenda, Sardinia (Italy)	Late Ordovician (Katian)	E	5
A40	9.376(2)	6.869(5)	*Scabbardella altipes* (Henningsmoen, 1948)	Cannamenda, Sardinia (Italy)	Late Ordovician (Katian)	E	5
A69	9.368(4)	6.885(8)	*Scabbardella altipes* (Henningsmoen, 1948)	Cannamenda, Sardinia (Italy)	Late Ordovician (Katian)	E	5
A70	9.373(2)	6.887(4)	*Scabbardella altipes* (Henningsmoen, 1948)	Cannamenda, Sardinia (Italy)	Late Ordovician (Katian)	E	5
A49	9.364(2)	6.884(3)	*Amorphognathus* sp. (Pa)	Saint-Hilaire-la-Gérard, Normandy (France)	Late Ordovician (Katian)	E	4-5
A50	9.367(3)	6.885(4)	*Amorphognathus* sp. (Pa)	Saint-Hilaire-la-Gérard, Normandy (France)	Late Ordovician (Katian)	E	4-5
A51	9.371(2)	6.884(2)	*Amorphognathus* sp. (Pa)	Saint-Hilaire-la-Gérard, Normandy (France)	Late Ordovician (Katian)	E	4-5
62	9.366(3)	6.887(3)	*Amorphognathus* sp. (Pb)	Saint-Hilaire-la-Gérard, Normandy (France)	Late Ordovician (Katian)	E	4-5
A52	9.371(2)	6.891(3)	*Amorphognathus* sp. (Pb)	Saint-Hilaire-la-Gérard, Normandy (France)	Late Ordovician (Katian)	E	4-5
A107	9.360(3)	6.887(3)	*Amorphognathus* sp. (Pb)	Saint-Hilaire-la-Gérard, Normandy (France)	Late Ordovician (Katian)	E	4-5
A108	9.364(3)	6.884(4)	*Amorphognathus* sp. (Pb)	Saint-Hilaire-la-Gérard, Normandy (France)	Late Ordovician (Katian)	E	4-5

17	9.357(4)	6.888(5)	*Amorphognathus* sp. (Sd)	Saint-Hilaire-la-Gérard, Normandy (France)	Late Ordovician (Katian)	E	4-5
68	9.379(2)	6.875(3)	*Hamarodus brevirameus* (Walliser, 1964) (M)	Saint-Hilaire-la-Gérard, Normandy (France)	Late Ordovician (Katian)	E	4-5
82	9.376(2)	6.880(3)	*Hamarodus brevirameus* (Walliser, 1964) (M)	Saint-Hilaire-la-Gérard, Normandy (France)	Late Ordovician (Katian)	E	4-5
49	9.365(2)	6.887(9)	*Hamarodus brevirameus* (Walliser, 1964) (Sc)	Saint-Hilaire-la-Gérard, Normandy (France)	Late Ordovician (Katian)	E	4-5
21	9.374(2)	6.880(2)	*Icriodella* sp.	Saint-Hilaire-la-Gérard, Normandy (France)	Late Ordovician (Katian)	E	4-5
20	9.374(4)	6.884(4)	*Panderodus* sp.	Saint-Hilaire-la-Gérard, Normandy (France)	Late Ordovician (Katian)	E	4-5
56	9.374(4)	6.867(6)	*Panderodus* sp.	Saint-Hilaire-la-Gérard, Normandy (France)	Late Ordovician (Katian)	E	4-5
A53	9.369(3)	6.878(6)	*Panderodus* sp.	Saint-Hilaire-la-Gérard, Normandy (France)	Late Ordovician (Katian)	E	4-5
24	9.369(2)	6.877(3)	*Sagittodontina robusta* Knüpfer, 1967 (Pa)	Saint-Hilaire-la-Gérard, Normandy (France)	Late Ordovician (Katian)	E	4-5
41	9.372(2)	6.886(5)	*Sagittodontina robusta* Knüpfer, 1967 (Pa)	Saint-Hilaire-la-Gérard, Normandy (France)	Late Ordovician (Katian)	E	4-5
46	9.368(6)	6.876(5)	*Sagittodontina robusta* Knüpfer, 1967 (Sd)	Saint-Hilaire-la-Gérard, Normandy (France)	Late Ordovician (Katian)	E	4-5
45	9.375(3)	6.884(5)	*Scabbardella altipes* (Henningsmoen, 1948)	Saint-Hilaire-la-Gérard, Normandy (France)	Late Ordovician (Katian)	E	4-5
59	9.375(4)	6.880(3)	*Scabbardella altipes* (Henningsmoen, 1948)	Saint-Hilaire-la-Gérard, Normandy (France)	Late Ordovician (Katian)	E	4-5
60	9.381(2)	6.881(2)	*Scabbardella altipes* (Henningsmoen, 1948)	Saint-Hilaire-la-Gérard, Normandy (France)	Late Ordovician (Katian)	E	4-5
91	9.368(2)	6.877(4)	*Scabbardella altipes* (Henningsmoen, 1948)	Saint-Hilaire-la-Gérard, Normandy (France)	Late Ordovician (Katian)	E	4-5
103	9.374(3)	6.908(4)	*Scabbardella altipes* (Henningsmoen, 1948)	Saint-Hilaire-la-Gérard, Normandy (France)	Late Ordovician (Katian)	E	4-5

A54	9.361(2)	6.906(5)	*Scabbardella altipes* (Henningsmoen, 1948)	Saint-Hilaire-la-Gérard, Normandy (France)	Late Ordovician (Katian)	E	4-5
A22	9.379(2)	6.889(2)	*Rhipidognathus symmetricus* Branson, Mehl and Branson, 1951	Saluda Dolomite (USA)	Late Ordovician	E	1
A23	9.363(3)	6.897(4)	*Panderodus* sp.	Saluda Dolomite (USA)	Late Ordovician	E	1
A104	9.374(3)	6.887(4)	*Belodina* sp.	Kimmswick Formation, Missouri (USA)	Late Ordovician	E	1
A105	9.359(3)	6.878(4)	*Plectodina* sp.	Kimmswick Formation, Missouri (USA)	Late Ordovician	E	1
A106	9.379(2)	6.886(4)	*Panderodus* sp.	Kimmswick Formation, Missouri (USA)	Late Ordovician	E	1
A1	9.368(4)	6.857(6)	*Zieglerodina planilingua* (Murphy & Valenzuela-Ríos, 1999)	U Topolů (Bohemia)	Early Devonian (Lochkovian)	E	3
A2	9.383(3)	6.885(3)	*Lanea omoalpha* (Murphy & Valenzuela-Ríos, 1999)	U Topolů (Bohemia)	Early Devonian (Lochkovian)	E	3
A82	9.370(3)	6.894(3)	*Palmatolepis* sp.	Pramosio A, Carnic Alps (Italy)	Late Devonian (Frasnian)	E	4.5
A83	9.376(2)	6.883(6)	*Polygnathus decorosus* Stauffer, 1938	Pramosio A, Carnic Alps (Italy)	Late Devonian (Frasnian)	E	4.5
A80	9.362(3)	6.886(4)	unrecognizable fragment	Casera Collinetta di Sotto A, Carnic Alps (Italy)	Late Devonian (Famennian)	E	4.5
A81	9.371(3)	6.881(6)	*Branmehla werneri* (Ziegler, 1957)	Casera Collinetta di Sotto A, Carnic Alps (Italy)	Late Devonian (Famennian)	E	4.5
A101	9.365(2)	6.878(3)	*Palmatolepis triangularis* Sannemann, 1955	Texas (USA)	Late Devonian (Famennian)	E	2
A102	9.384(1)	6.886(2)	*Palmatolepis subperlobata* Branson and Mehl, 1934	Texas (USA)	Late Devonian (Famennian)	E	2
A103	9.378(2)	6.879(3)	*Icriodus* sp.	Texas (USA)	Late Devonian (Famennian)	E	2
A76	9.377(2)	6.871(3)	unrecognizable fragment	Dolina, Carnic Alps (Italy)	Carboniferous Early Mississippian (Tournaisian)	E	4.5

A77	9.356(2)	6.882(2)	unrecognizable fragment	Dolina, Carnic Alps (Italy)	Carboniferous Early Mississippian (Tournaisian)	E	4.5
A100	9.370(2)	6.882(3)	unrecognizable fragment	Dolina, Carnic Alps (Italy)	Carboniferous Early Mississippian (Tournaisian)	E	4.5
A78	9.374(2)	6.884(3)	*Gnathodus* sp.	Dolina, Carnic Alps (Italy)	Carboniferous Middle Mississippian (Visean)	E	4-4.5
A79	9.370(2)	6.887(4)	*Gnathodus* sp.	Dolina, Carnic Alps (Italy)	Carboniferous Middle Mississippian (Visean)	E	4-4.5
A86	9.374(2)	6.878(3)	*Pachycladina obliqua* Staesche, 1964	Cencenighe Galleria, Dolomites (Italy)	Early Triassic (Olenekian)	E	5.5-6
A87	9.363(2)	6.904(5)	*Pachycladina obliqua* Staesche, 1964	Cencenighe Galleria, Dolomites (Italy)	Early Triassic (Olenekian)	E	5.5-6
A84	9.355(3)	6.888(3)	unrecognizable fragment	Sotto le Rive, Dolomites (Italy)	Middle Triassic (Anisian)	E	1.5
A85	9.362(4)	6.881(5)	unrecognizable fragment	Sotto le Rive, Dolomites (Italy)	Middle Triassic (Anisian)	E	1.5
A42	9.372(2)	6.884(2)	*Carnepigondolella pseudodiebeli* (Kozur, 1972)	Pizzo Mondello, Sicani Mountains, Sicily (Italy)	Late Triassic (Carnian)	E	1.5
A43	9.383(3)	6.883(4)	*Carnepigondolella pseudodiebeli* (Kozur, 1972)	Pizzo Mondello, Sicani Mountains, Sicily (Italy)	Late Triassic (Carnian)	E	1.5
A44	9.382(2)	6.881(3)	*Carnepigondolella pseudodiebeli* (Kozur, 1972)	Pizzo Mondello, Sicani Mountains, Sicily (Italy)	Late Triassic (Carnian)	E	1.5

Table SI-1b. Bioapatite cell parameters calculated for other phosphatic/phosphatized fauna.

Code	*a* (Å)	*c* (Å)	Taxa	Locality/Formation	Age
A16	9.356(4)	6.900(4)	ostracod	Kinnekulle, Västergötland (Sweden)	Cambrian Furongian (Paibian)
A17	9.353(4)	6.903(3)	ostracod	Kinnekulle, Västergötland (Sweden)	Cambrian Furongian (Paibian)
A92	9.349(4)	6.900(3)	ostracod	Kinnekulle, Västergötland (Sweden)	Cambrian Furongian (Paibian)
A93	9.346(6)	6.908(6)	ostracod	Kinnekulle, Västergötland (Sweden)	Cambrian Furongian (Paibian)
A94	9.338(7)	6.885(7)	ostracod	Kinnekulle, Västergötland (Sweden)	Cambrian Furongian (Paibian)
A95	9.358(5)	6.905(4)	undetermined	Kinnekulle, Västergötland (Sweden)	Cambrian Furongian (Paibian)
A96	9.345(2)	6.909(3)	undetermined	Kinnekulle, Västergötland (Sweden)	Cambrian Furongian (Paibian)
A97	9.356(6)	6.899(4)	undetermined	Kinnekulle, Västergötland (Sweden)	Cambrian Furongian (Paibian)
A7	9.354(1)	6.887(2)	brachiopod	Öland (Sweden)	Early Ordovician (Tremadocian)
A8	9.335(5)	6.887(5)	brachiopod	Öland (Sweden)	Early Ordovician (Tremadocian)
A25	9.367(2)	6.892(2)	brachiopod	Keisley, Westmorland (UK)	Late Ordovician (Katian)
A26	9.368(3)	6.892(3)	brachiopod	Keisley, Westmorland (UK)	Late Ordovician (Katian)
A73	9.366(2)	6.880(2)	brachiopod	Cannamenda, Sardinia (Italy)	Late Ordovician (Katian)
A36	9.362(2)	6.888(2)	brachiopod	Cannamenda, Sardinia (Italy)	Late Ordovician (Katian)
A55	9.337(3)	9.868(3)	brachiopod	Saint-Hilaire-la-Gérard, Normandy (France)	Late Ordovician (Katian)
A64	9.372(2)	6.890(2)	brachiopod	Saint-Hilaire-la-Gérard, Normandy (France)	Late Ordovician (Katian)
A3	9.343(3)	6.897(3)	brachiopod	U Topolů (Bohemia)	Early Devonian (Lochkovian)
A4	9.345(3)	6.891(3)	brachiopod	U Topolů (Bohemia)	Early Devonian (Lochkovian)
A35	9.365(1)	6.896(2)	bryozoan	Cannamenda, Sardinia (Italy)	Late Ordovician (Katian)
A71	9.351(2)	6.884(4)	bryozoan	Cannamenda, Sardinia (Italy)	Late Ordovician (Katian)
A58	9.368(3)	6.889(3)	bryozoan	Saint-Hilaire-la-Gérard, Normandy (France)	Late Ordovician (Katian)

A61	9.371(2)	6.891(2)	bryozoan	Saint-Hilaire-la-Gérard, Normandy (France)	Late Ordovician (Katian)
A65	9.372(3)	6.887(4)	bryozoan	Saint-Hilaire-la-Gérard, Normandy (France)	Late Ordovician (Katian)
A24	9.361(2)	6.893(3)	bryozoan	Saluda Dolomite (USA)	Late Ordovician
A45	9.337(3)	6.901(3)	fish tooth	Pizzo Mondello, Sicani Mountains, Sicily (Italy)	Late Triassic (Carnian)
A46	9.343(5)	6.896(4)	fish tooth	Pizzo Mondello, Sicani Mountains, Sicily (Italy)	Late Triassic (Carnian)
A47	9.411(6)	6.881(5)	fish tooth	Pizzo Mondello, Sicani Mountains, Sicily (Italy)	Late Triassic (Norian)